JOURNAL OF GEOPHYSICAL RESEARCH, VOL. 105, NO. D8, PAGES 10,081–10,102, APRIL 27, 2000

Boundary layer evolution and regional-scale diurnal circulations over the Mexico Basin and Mexican plateau

C. D. Whiteman, S. Zhong, X. Bian, J. D. Fast, and J. C. Doran

Pacific Northwest National Laboratory, Richland, Washington

Abstract. Data collected in a measurement campaign in February and March 1997 showed that the Mexico Basin (also called the Valley of Mexico), located atop the Mexican plateau, fails to develop the strong nocturnal inversions usually associated with basins and does not exhibit diurnally reversing valley wind systems. Data analyses, two- and three-dimensional numerical simulations with the Regional Atmospheric Modeling System (RAMS), and a Lagrangian particle dispersion model are used to interpret these observations and to examine the effects of topography and regional diurnal circulations on boundary layer evolution over the Mexico Basin and its surroundings during fair weather periods in the winter dry season. We show that the boundary layer evolution in and above the basin is driven primarily by regional diurnal circulations that develop between the air above the Mexican Plateau and the generally cooler surrounding coastal areas. A convective boundary layer (CBL) grows explosively over the plateau in the late morning to reach elevations of 2250 m agl (4500 m msl) by noon, and a strong baroclinic zone forms on the edges of the plateau separating the warm CBL air from its cooler surroundings. In early afternoon the rates of heating and CBL growth are slowed as cool air leaks onto the plateau and into the basin through passes and over low-lying plateau edges. The flow onto the plateau is retarded, however, by the strongly rising branch of a plain-plateau circulation at the plateau edges, especially where mountains or steep slopes are present. An unusually rapid and deep cooling of the air above the plateau begins in late afternoon and early evening when the surface energy budget reverses, the CBL decays, and air accelerates onto the plateau through the baroclinic zone. Flow convergence near the basin floor and the associated rising motions over the basin and plateau produce cooling in 3 hours that is equivalent to half the daytime heating. While the air that converges onto the plateau comes from elevations at and above the plateau, it is air that was modified earlier in the day by a cool, moist coastal inflow carried up the plateau slopes by the plain-plateau circulation.

1. Introduction

The geographical setting of basin topography, high altitude, and tropical latitude, combined with high population density and multiple emission sources, makes Mexico City and its immediate surroundings one of the most polluted areas of the world. The basin setting inhibits pollution dispersion, and intense year-around sunshine at this latitude and elevation promotes atmospheric photochemical reactions that form secondary pollutants such as ozone. As a result, ozone values up to 400 ppb have been measured in the basin, and the Mexico air quality standards are frequently exceeded at many locations in and around the urban complex [*Garfias and Gonzalez*, 1992; *Collins and Scott*, 1993].

While many air quality studies have been carried out in the Mexico City area using surface measurements from an automated monitoring network [*Raga and Le Moyne*, 1996; *Miller et al.*, 1994; *Garfias and González*, 1992; *Bravo et al.*, 1996; *Bian et al.*, 1998], upper air observations from aircraft flights [*Nickerson et al.*, 1992; *Díaz-Francés et al.*, 1994], and photochemical models [*Varela*, 1994; *Fast*, 1999], few studies have attempted to describe the meteorology of this elevated basin, and those that are available in the literature rely heavily on surface observations. In a series of studies using data from surface meteorological stations in urban and rural areas of the basin, *Jauregui* [1973, 1988, 1993, 1997] documented the urban climatology of Mexico City, especially the heat island development and its associated local circulations. *Oke et al.* [1992, 1999] reported investigations of surface energy budget components in heavily built-up areas of Mexico City and compared them to components at similar sites in temperate cities. This was one of the first such studies in a tropical urban area.

In recent years, two major research programs have carried out field campaigns in Mexico City and its surroundings to provide badly needed upper air meteorological observations. The first of these was the Mexico City Air Quality Research Initiative (MARI) conducted in the winters of 1990-1993 as a cooperative study between Los Alamos National Laboratory and the Mexico Petroleum Institute [*Guzmán and Streit*, 1993]. *Williams et al.* [1995] used the MARI data to perform mesoscale model simulations of local circulations and dispersion in the Mexico City area for several selected cases and to evaluate sources of uncertainty by using model-measurement comparisons. *Bossert* [1997] used a mesoscale model to simulate the observed wind and temperature structures on three days during the MARI field experiment in February

Paper number 2000JD900039.
0148-0227/00/2000JD900039$09.00

1991 to examine how they affect observed pollutant concentrations. He concluded that both regional- and synoptic-scale flows have a strong effect on the meteorology and air pollution concentrations within the Mexico Basin. The second research program, the Investigation sobre Materia Particulada y Deterioro Atmosferico-Aerosol and Visibility Research (IMADA-AVER), was conducted during the period February 23 through March 22, 1997, and was funded jointly by Petróleos Mexicanos through the Instituto Mexicano del Petróleo and the U.S. Department of Energy [*Doran et al.*, 1998]. The IMADA program obtained improved data on the spatial patterns of aerosols in Mexico City [*Edgerton et al.* 1999] and improved spatial information on the evolution of vertical wind and temperature structure in the Mexico Basin. *Fast and Zhong* [1998] used data from this experiment to link boundary layer circulation patterns to the observed spatial ozone distribution patterns in the basin by studying seven pollution episodes during the IMADA-AVER experiment using a high-resolution mesoscale meteorological model and a Lagrangian particle dispersion model. Their simulations showed that the day-to-day distribution of pollutants within the Mexico Basin was rather sensitive to small changes in upper level wind speed and direction that affected the diurnal cycle of winds in the basin.

Although the above mentioned studies have provided valuable new information on meteorological processes in the Mexico City area, they have focused primarily on the linkage between meteorology and air quality within the basin and are therefore limited in spatial extent and to selected case studies of high-pollution episodes. The present paper complements these studies by focusing on the characteristics of mean temperature and wind structure evolution in the elevated basin using data from a special network of radar profilers and radiosonde stations operated during the IMADA-AVER experimental period and from the Mexican rawinsonde network stations within and surrounding the elevated basin. Data from these sources were composited to elucidate the regular diurnal patterns of boundary layer evolution. Numerical model simulations were used to interpret the observations and to determine the effect of topography and regional-scale diurnal circulations on boundary layer structure evolution within the Mexico Basin.

Section 2 describes the topographic setting of the basin. Section 3 provides information on the experimental sites and data, as well as the synoptic weather conditions. Section 4 presents analyses of the observed boundary layer structure and evolution. Model simulations are presented in section 5. This is followed by discussions in section 6 and conclusions in section 7.

2. Mexico Basin

The topography (Figure 1) surrounding Mexico City has been described variously as that of a basin, a valley, and a plateau. The Mexico City metropolitan area (latitude 19°N) is found in the southwestern portion of the broad Mexico Basin. The nearly flat floor of the basin (elevation 2250 m mean sea level (msl)) is confined on three sides by mountain ridges but with a broad opening to the north and a narrower gap or pass to the south-southeast. The surrounding ridges vary in elevation, but the basin can be considered roughly 800-1000 m deep. Two high snow-covered volcanoes (Popocatépetl,

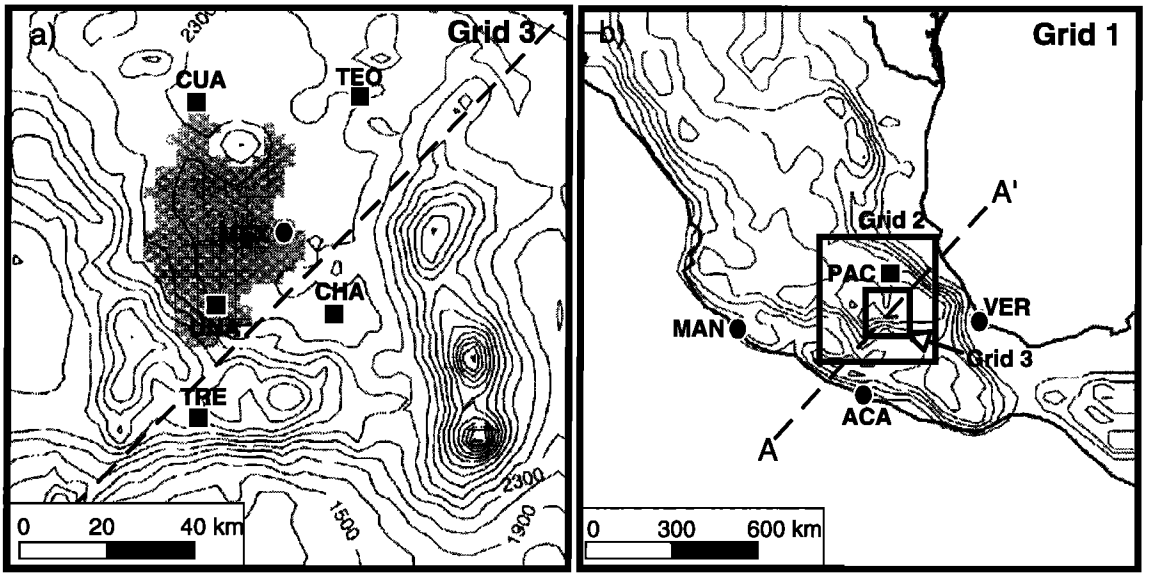

Figure 1. Topography of Mexico. (a) Map of the Mexico Basin, showing the locations of the Investigation sobre Materia Particulada y Deterioro Atmosferico-Aerosol and Visibility Research (IMADA-AVER) radar profiler/ radiosonde sites (squares), the Mexico City airport rawinsonde site (dot), and the Mexico City metropolitan area (shaded). The topographic contour interval is 200 m. (b) Three coastal Mexican rawinsonde sites (dots), a GPS rawinsonde site (square), the three nested Regional Atmospheric Modeling System (RAMS) simulation grids, and the cross-section A-A' through the isthmus used in two-dimensional model simulations. The topographic contour interval is 500 m. Site abbreviations are as follows: ACA, Acapulco; CHA, Chalco; CUA, Cuautitlan; MAN, Manzanillo; MEX, Mexico City International Airport; PAC, Pachuca; TEO, Teotihuacan; TRM, Tres Marias; UNA, UNAM; VER, Veracruz.

5452 m, and Iztaccihuatl, 5286 m) are found on the mountain ridge southeast of the basin. The gap to the south-southeast of the basin, when combined with the opening to the north, has led to descriptions of the topography as being that of a broad valley (Valle de México). The basin and its surrounding mountains are located at the south end of a large plateau (the Mexican plateau) which occupies the center of the Mexican isthmus. The outer slopes of this plateau to the west fall to the Pacific Ocean, while those to the east descend to the Atlantic Ocean. The unusual multiscale topographic complexity of this region raises the question whether the boundary layer development of this area will be primarily like that of a valley, a basin, or a plateau.

3. Sites, Data, and Synoptic Overview

The air quality and meteorological data collected during the IMADA-AVER field campaign were described by *Doran et al.* [1998]. Only the surface and upper air meteorological data used in this paper are summarized here. Hourly wind profiles from four 915 MHz radar wind profilers located within the basin at Teotihuacan (TEO), Cuautitlan (CUA), Universidad Nacional Autónoma (UNA) de México (UNAM), and Chalco (Figure 1a) were used to sample the above-basin wind field. The profilers were operated in both low- and high-range modes with vertical resolutions of 60 and 100 m and covered a height range of approximately 100 - 2000 m and 150 - 4000 m above ground level (agl), respectively. The temperature structure evolution in the basin was determined from radiosonde soundings launched 5 times per day (0800, 1100, 1330, 1630, 1930 local standard time (LST)), except on Sundays, from these four profiler sites. Temperature and humidity profiles to the north and south of the basin were determined from radiosonde soundings at two additional sites: Pachuca, located approximately 70 km northeast of Mexico City, and Tres Marias, located on the southern flank of the mountains forming the southern boundary of the basin. Soundings were launched at 1330, 1630, and 1930 LST at Pachuca and at 1330 and 1630 LST at Tres Marias. Twice-daily soundings launched at 0600 and 1800 LST from the Mexican national rawinsonde network were used to provide information on regional-scale atmospheric conditions within and surrounding the Mexico Basin.

Table 1. Station Locations and Data Types

Station	ID	Lat (°N)	Long (°W)	Elev (m)	Data
Chalco	CHA	19.25	98.91	2248	R, P
Cuautitlan	CUA	19.69	99.19	2252	R, P
Teotihuacan	TEO	19.68	98.85	2275	R, P
UNAM	UNA	19.32	99.19	2274	R, P
Acapulco	ACA	16.05	99.93	3	R/S
Manzanillo	MAN	19.07	104.33	3	R/S
Veracruz	VER	19.17	96.12	13	R/S
Mexico City Int'l Airport	MEX	19.43	99.07	2234	R/S
Tres Marias	TRE	19.05	99.45	2810	R1
Pachuca	PAC	20.08	98.74	2425	R2

R, radiosondes launched at 0800, 1100, 1330, 1630, and 1930 LST; R1, radiosondes launched at 1330 and 1630 LST; R2, Global Positioning System rawinsondes launched at 1430, 1630, and 1930 LST; R/S, rawinsondes launched at 0600 and 1800 LST; P, 915 MHz radar wind profiler (hour-average data).

Table 2. February-March 50 kPa Geopotential Heights, Temperatures, Dew Points, and Wind Speeds, as Averaged Over a 10-year Period (1988-1997) and for 1997

	10-year February-March Average		1997 February-March Average	
	0000 UTC	1200 UTC	0000 UTC	1200 UTC
Geopotential height (m)	5859	5854	5861	5859
Temperature (°C)	-8.8	-7.9	-8.7	-8.1
Dew point temperature (°C)	-22.1	-29.5	-22.8	-31.0
Wind speed (m/s)	8.6	10.6	8.0	10.7

Network soundings were made from the Mexico City International Airport inside the basin and at three coastal sites outside the basin (Figure 1b), one south of the basin at Acapulco, one east of the basin at Veracruz, and one west of the basin at Manzanillo. There was no suitable representative rawinsonde station north of the basin. Table 1 summarizes information on the sites and the types of data collected.

The experimental period was near the end of the winter dry season. The synoptic conditions during this period were characterized by high pressure with light upper level winds and near-cloudless skies. Partially cloudy skies and some precipitation occurred on a few days at the beginning of the experiment when a deep trough was found over New Mexico and Texas with its influence extending southward to northcentral Mexico and toward the end of the experiment when a cutoff low formed off the Pacific coast of central Mexico.

To determine the representativeness of the general synoptic conditions occurring during the experimental period, rawinsonde data from the Mexico City International Airport were used to determine mean values of geopotential height, temperature, dew point temperature, and wind speed at 70 and 50 kPa for February and March for the years 1988-1997. A comparison of these climatological mean values with the same variables averaged over February and March 1997 is shown in Table 2. Because no significant differences occurred between the 1997 mean values and those averaged over 10 years, the upper air conditions during the 1997 IMADA-AVER field campaign are considered typical for the winter dry season in this region.

4. Observed Characteristics of Boundary Layer Evolution

4.1. Mean Temperature and Humidity Structure

Radiosonde temperature data were composited from all days of the experimental period (February 23 through March 22, 1997) for three of the four basin sites (TEO, CUA, and UNA) to obtain mean temperature profiles at the five daily sounding times. Missing data from the Chalco site precluded a similar treatment there. Figure 2 shows the diurnal variation of the mean temperature structure at Teotihuacan, UNAM, and Chalco. Because of missing soundings, the data composites at the three sites use data from different experimental days. Because of this the time evolution of potential

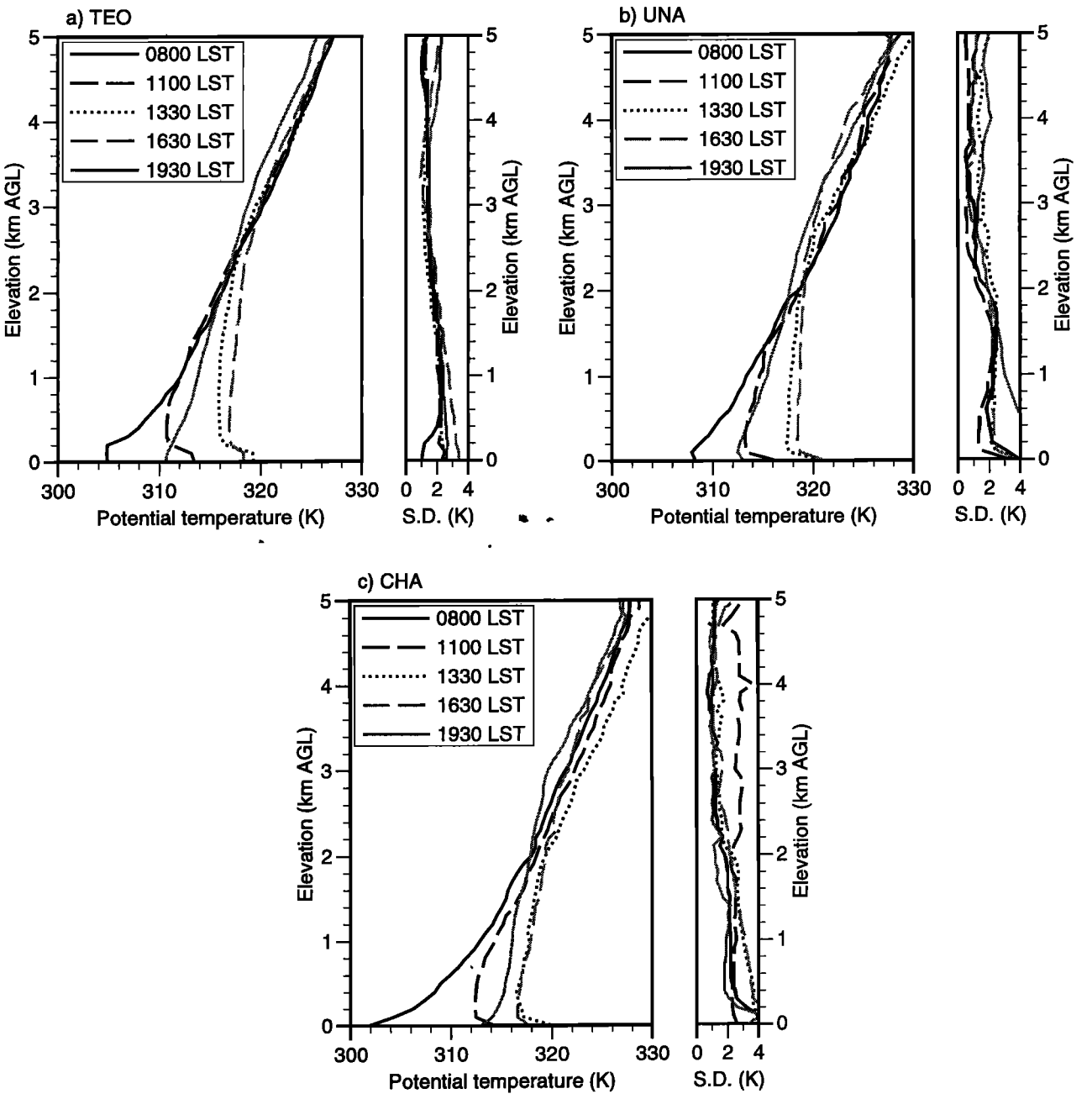

Figure 2. Mean radiosonde soundings at (a) Teotihuacan, (b) UNAM, and (c) Chalco. Each sounding is a composite of all good-quality soundings (typically 19-23) in the February 23 to March 22, 1997, experimental period for the time (local standard time (LST)) indicated. The composite profiles are constructed from individual soundings whose temperatures are averaged over 100-m vertical segments. The standard deviations (s.d.) of mean potential temperatures as averaged over 100-m vertical segments in the individual soundings are shown in figure parts for the times indicated.

temperature at a site is expected to be more accurate than comparisons between sites. While the atmospheric boundary layer in the Mexico Basin evolves normally in several respects, it also exhibits some unusual features, which will be discussed for the Teotihuacan site (Figure 2a). The mixed layer at Teotihuacan goes through a rapid growth period between 1100 and 1330 LST, attaining a depth that exceeds 2000 m agl (4250 m msl) by 1330 LST. Between 1330 and 1630 LST the rate of growth of boundary layer depth and the rate of boundary layer warming slow significantly. Most peculiarly, a very sudden cooling occurs throughout the entire boundary layer to an elevation of 2250 m agl (4500 m msl) between the 1630 and 1930 LST soundings. The cooling during this 3-hour period is equivalent in value to more than half of the total daytime heating! The main features of boundary layer development at the rural Teotihuacan site were also present at the urban UNAM (Figure 2b) and rural Chalco (Figure 2c) sites. At the Chalco site, almost no warming

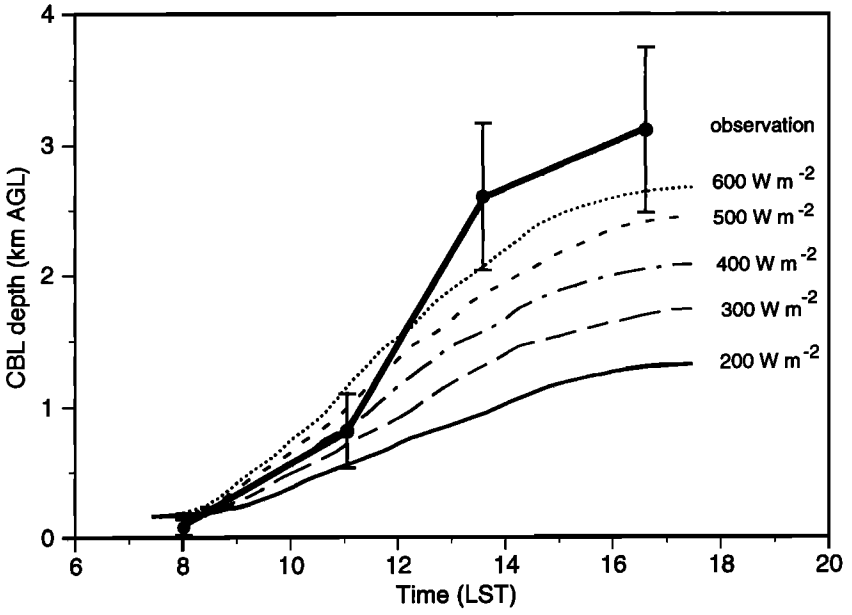

Figure 3. Mean (dots) and standard deviations (error bars) of observed convective boundary layer (CBL) depths at Teotihuacan. Also shown are CBL depths estimated with a simple encroachment model given sinusoidal surface sensible heat fluxes with the indicated amplitudes using the mean 0800 LST sounding as an initial condition.

occurred between 1330 and 1630 LST, the cooling between 1630 and 1930 LST was reduced relative to the other sites, and a shallow ground-based cold air layer was present in the 0800 LST sounding. The standard deviations of sounding temperatures for each of the sounding times are shown in Figure 2 to quantify the day-to-day variability in boundary layer temperatures at the individual sites. Standard deviations were generally less than 2 K above 2000 m agl, except for the 1000 LST soundings at Chalco. The standard deviations increased below this level, exceeding 4 K at the ground for several of the afternoon and evening soundings.

The daytime boundary layer growth in the Mexico Basin can be seen more clearly in Figure 3. Here the means and standard deviations of boundary layer heights are plotted as a function of time for Teotihuacan. The means and standard deviations were determined subjectively from individual potential temperature soundings by recording the height of the base of the capping inversion at the top of the unstable or convective boundary layer (CBL). Also plotted in Figure 3 are the hypothetical rates of boundary layer growth calculated from an encroachment model using the mean 0800 LST Teotihuacan sounding as the initial sounding and assuming sinusoidally varying surface sensible heat fluxes between sunrise and sunset with maximum values at solar noon ranging from 200 to 600 W m^{-2}. The encroachment model neglects advection, subsidence, and turbulent entrainment but is nonetheless generally considered a useful tool in estimating boundary layer depths over homogeneous terrain and has been shown to explain 80-90% of the observed variations in boundary layer depth [*Stull*, 1988]. The plot shows a rapid increase of boundary layer depth between 1100 and 1330 LST, with an average growth rate exceeding 600 m per hour, much larger than the rate suggested by the encroachment model. After 1330 LST the growth rate fell off steeply in comparison to its earlier rate of growth, attaining a rate similar to that predicted by the encroachment model with a maximum mid day flux of 400 Wm^{-2}.

Regular diurnal circulations form in areas of complex terrain when horizontal air temperature differences occur between locations within the mountainous area or between the air over the topography and the air over the surrounding plain. These temperature differences lead to horizontal pressure gradients that drive diurnal mountain wind systems [*Whiteman*, 1990]. Therefore as a first step in investigating diurnal wind systems, analyses of horizontal temperature differences were performed on different scales.

The spatial variation of mixed layer temperatures within the basin, as determined from the four basin sites during the experimental period, is usually small and variable from day to day, so no consistent patterns were detected except for a tendency for slightly cooler (0.5-1 K) afternoon temperatures at Chalco. Some differences, however, exist between the mixed layer temperatures and the boundary layer structure inside the basin and those south and north of the basin. At Pachuca the 3 times per day soundings are much like the soundings from the four stations in the Mexico Basin (not shown). Boundary layer depths and temperatures are similar and they also show the suppressed boundary layer development between 1330 to 1630 LST and the rapid decay and cooling between 1630 and 1930 LST. South of the basin at the higher altitude site of Tres Marias, the twice-daily soundings at 1330 and 1630 LST exhibit shallower mixed layers and cooler temperatures than at the other sites. Figure 4 illustrates these differences by plotting the mean potential temperature soundings at 1630 LST at UNAM, Pachuca, and Tres Marias. The afternoon temperatures are generally warmer inside the basin, with the UNAM-Tres Marias temperature difference larger than the UNAM-Pachuca temperature difference. The warmer temperatures within the basin are consistent with the frequently observed afternoon flows that enter

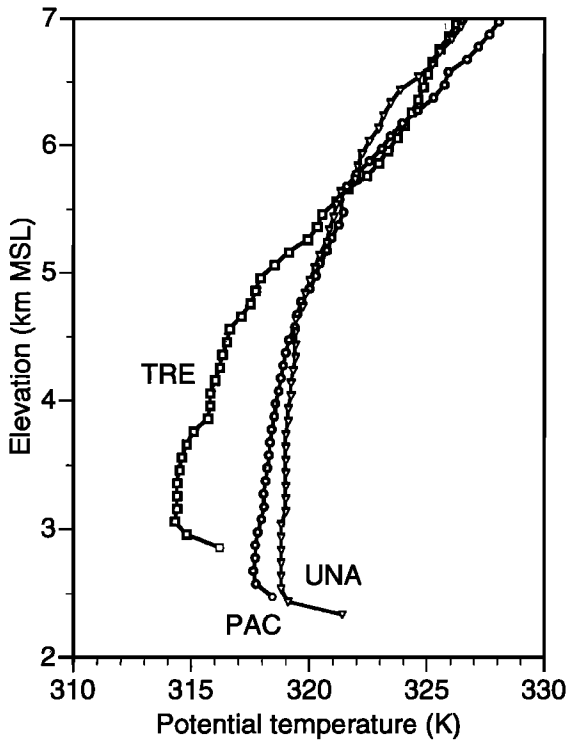

Figure 4. Mean potential temperature soundings at 1630 LST at UNAM, Pachuca, and Tres Marias. Soundings are averaged from all available soundings (12 at TRE, 20 at PAC, and 22 at UNA) at the 1630 observation time during the February 23 to March 22, 1997, experimental period.

the basin from the south-southeast at Chalco and from the north-northeast at Teotihuacan and Cuautitlan, as will be discussed later.

A comparison was also made between Mexico Basin temperature and mixing ratio profiles and profiles obtained from the coastal regions surrounding the Mexican plateau. Mean potential temperature and mixing ratio soundings for the period from February 1 to March 31, 1997, were constructed for 0600 (Figures 5a and 5c) and 1800 LST (Figures 5b and 5d) for each of the four Mexican rawinsonde stations (see Figure 1b for locations).

At 0600 LST, after a full night's cooling, the basin floor experiences a slight potential temperature deficit relative to the surrounding coastal stations (Figure 5a). The deficit near the basin floor is about 3 K relative to air at the same height above Manzanillo and Acapulco but only about 1 K relative to Veracruz. The temperature deficit decreases with altitude above the basin floor. The mean vertical potential temperature gradient above the plateau level at all rawinsonde sites is about 0.0043 K m^{-1}, slightly larger than that of the midlatitude Standard Atmosphere (0.0035 K m^{-1}). Below the altitude of the plateau, soundings on the Atlantic side of the Isthmus were up to 4 K colder than on the Pacific side. The small temperature difference between the atmosphere inside and outside the basin at altitudes between 2250 and 3250 m msl is not consistent with observations in other basins and valleys, which are generally characterized by cold air confinement at night and large temperature deficits relative to their surroundings [*Whiteman et al.*, 1996, 1999a, 1999b]. Others [e.g., *Collins and Scott*, 1993] have stated that air quality problems in the Mexico Basin are exacerbated by strong temperature inversions that form within the elevated basin. The mean potential temperature sounding at the Mexico City airport, however, shows no temperature inversion (a temperature inversion would require $d\theta/dz > 0.0098$ K m^{-1}). In fact, the mean morning low-level stability is only marginally greater than in the free atmosphere surrounding the Mexican plateau at the same altitude. While the atmosphere over the basin is stable at night and actual temperature inversions formed occasionally during the experimental period, the Mexico Basin has lower mean nighttime stability than most midlatitude Rocky Mountain valleys and basins [*Whiteman et al.*, 1999b]. In these valleys, mean potential temperature gradients in the surface-based inversion near sunrise following clear nights usually exceed 0.015 K m^{-1}. In this sense, the Mexico Basin does not exhibit one of the chief meteorological characteristics of basins, the formation of strong nighttime temperature inversions.

The mixing ratio profiles at 0600 LST (Figure 5c) at the Mexico City airport, Veracruz, and Acapulco were nearly identical above the altitude of the Mexican plateau, while the profile above Manzanillo was drier. Mixing ratios at sea level in the coastal areas on either side of the plateau were nearly double those on the Mexican plateau. The highest mixing ratios were confined to an 800-m-deep layer on the Pacific side of the Isthmus at Acapulco, whereas the mixing ratio decreased linearly with elevation above Veracruz on the Atlantic side.

At 1800 LST a deep CBL (Figure 5b) extends to 4600 m msl above the basin, as determined from soundings at the Mexico City airport. At the other sites, however, the soundings have much the same appearance as at 0600 LST, although they are somewhat warmer (by 0-4 K) than the morning soundings in the lowest 4000 m. A slight destabilization in the lowest 200-400 m at Acapulco, Manzanillo, and Veracruz is associated with the development of shallow CBLs there. The CBL above the elevated Mexico Basin is much deeper (and warmer) than CBLs in coastal areas on either side of the isthmus. The temperature difference between the basin site and the other sites decreases linearly from an excess of 8-10 K at the basin floor to a deficit of 1.5 to 3.5 K at 4700 m msl. Hence the basin atmosphere above the 4300 m msl is colder than its surroundings. The overheating of the atmosphere within and above the basin relative to the coastal environment is clearly produced by the daytime growth of a deep CBL above the basin floor. The strong daytime overheating associated with CBL growth over the basin and plateau is in contrast to the weak nighttime overcooling of the basin atmosphere. While the radiosonde observations lack temporal resolution, it is clear from the Teotihuacan observations that the large daytime overheating dissipates very rapidly in the late afternoon and early evening, leaving only a weak overcooling in the basin by the 0600 LST soundings.

The mixing ratio profiles (Figure 5d) at 1800 LST above the elevation of the Mexican plateau change little from the morning profiles, except at the MEX site, where the humidity is mixed through the deep CBL above the plateau, with significant moistening at altitudes between 3800 and 6000 m msl. At the altitude of the basin floor, the humidity is slightly lower than at the same altitude over Veracruz but slightly higher than in the mixed layer above. The mean mixing ratio above the plateau between the surface and 7300 m msl, the altitude where day/night differences become negligible, is

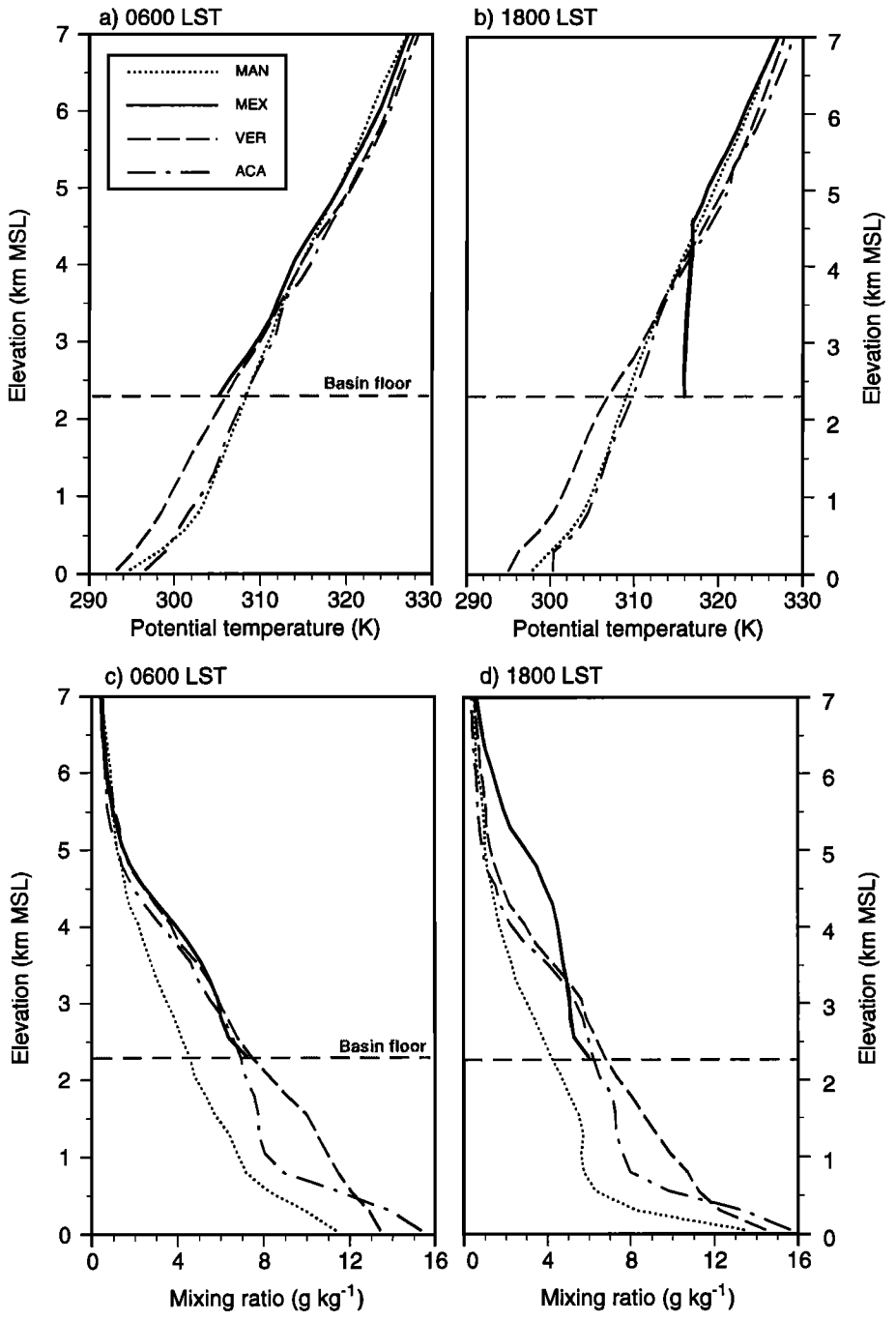

Figure 5. Mean potential temperature profiles at (a) 0600 and (b) 1800 LST and mixing ratio profiles at (c) 0600 and (d) 1800 LST at Manzanillo, Mexico City International Airport, Veracruz, and Acapulco, as averaged over the period February 1 through March 31, 1997.

2.8 g kg^{-1} at 0600 LST and 3.1 g kg^{-1} at 1800 LST. Thus a net increase in humidity occurs above the plateau during the daytime growth of the mixed layer. Since there are no large moisture sources on the plateau itself and the growing CBL would entrain lower humidity air into the mixed layer, the observations suggest that advection from the surrounding coastal regions is responsible for this moistening. Some of the additional moisture is, no doubt, brought up from the more humid coastal regions by upslope flows that form during daytime on the outer slopes of the plateau.

In summary, the daytime boundary layer evolution above the Mexico Basin is characterized by a rapid heating and growth stage between 1100 and 1330 LST, followed by a quenching stage between 1330 and 1630 LST in which the rate of heating and growth slow, and an unusually rapid and deep cooling stage from 1630 to 1930 LST, with 3-hour cooling amounting to more than half of the total daytime heating. The air above the basin is significantly warmer in daytime relative to the large-scale environment as a result of CBL growth above the elevated basin floor. In contrast, the night-

time temperature deficit in the basin is small, so the potential temperature profile in the basin in the early morning differs little from profiles over the coastal stations on either side of the isthmus.

4.2. Energetics of the Mexico Basin Atmosphere

Changes in basin boundary layer temperature and depth can be investigated by calculating the rate of change of heat storage in the basin atmosphere from the equation

$$H = c_p \int_0^{z_m} \rho \frac{\Delta\theta}{\Delta t} dz \qquad [\mathrm{Wm^{-2}}] \qquad (1)$$

where c_p is the specific heat of air at constant pressure, ρ is air density, θ is potential temperature, t is time, and z is height. Increases in atmospheric heat storage, as calculated from equation (1), are produced by convergence of turbulent sensible and radiative heat fluxes and by advection [e.g., *Whiteman*, 1990]. In clear atmospheres over flat terrain during daytime, the contribution of radiative flux convergence to the gain of atmospheric heat storage is typically small compared to turbulent sensible heat flux convergence. During nighttime, radiative and turbulent sensible heat flux divergences may both play important roles leading to atmospheric heat loss [e.g., *Stull*, 1988]. Large discrepancies between measured surface sensible heat fluxes and rates of change in atmospheric heat storage are usually caused by advection associated with mean winds. In fact, in midlatitudes, advection associated with traveling extratropical cyclones causes large day-to-day variations in calculated heat storage rates. Because the Mexico Basin is in a quiescent tropical synoptic-scale environment, day-to-day variations in heat storage rate due to advection are expected to be small relative to midlatitude environments. Further, because air temperatures above the Mexico Plateau become more or less equilibrated with temperatures surrounding the plateau at night (Figure 5), large-scale advection is not expected to be important during much of the night. During the afternoon when the atmosphere over the plateau becomes warmer than its surroundings, any advection is expected to be cold air advection, which would decrease the atmospheric heat storage over the plateau.

Equation (1) was evaluated from potential temperature differences over 100-m height intervals from pairs of consecutive potential temperature soundings. The integration was performed to z_m=3000 m agl in order to extend above the daytime CBLs. The results, averaged over the 4-week experiment period, which was composed mostly of clear days or clear days with scattered cloudiness in the late afternoon, are plotted in Figure 6 at the midpoint times between soundings. Also plotted in Figure 6, for comparison purposes, are extraterrestrial solar radiation from a solar model [*Whiteman and Allwine*, 1986] and the measured total incoming solar and net all-wave radiation at UNAM on March 1, 1997. The mean rates of heat storage at the four sites in the basin differ by several hundred watts per meter squared during the period from midafternoon through early evening. Nonetheless, the rates of change of heat storage at all four sites show a consistent diurnal pattern, represented by the dashed curve in Figure 6. The curve rises rapidly in the morning, following the sinusoidal net radiation curve closely between 0800 and 1330 LST, attaining 550 W m^{-2} in midday. In the afternoon, however, it falls more rapidly than the net radiation curve, exhibiting a distinct diurnal asymmetry. The falloff of the rate of heat storage from the net radiation curve in the afternoon, indicated by hatched shading, could be interpreted as a quenching of boundary layer growth caused by the leakage of cold air into the warm basin atmosphere from the colder surroundings. The rate of heat loss from 1630 to 1930 LST reaches 450 W m^{-2}. This rate is much larger than typical valley or basin turbulent sensible heat flux divergences at this time of day. *Whiteman et al.* [1996], for example, showed measured and calculated (from an atmospheric heat budget) evening and nighttime sensible heat flux divergences from a Japanese basin, a Colorado valley, and a Colorado/Utah basin which were equivalent to surface sensible heat flux losses at rates generally less than 40 W m^{-2}. Cold air advection (i.e., divergence of potential temperature flux by the mean wind) must be invoked to explain the extremely high rates of heat loss over the Mexico Basin. The overnight cooling rate between 1930 and 0800 LST, although much smaller than during the afternoon and evening period, occurs at a rate comparable to what would be produced if all the net radiative loss at the surface were converted to sensible heat flux divergence in the column. A further discussion of these results in terms of mechanisms that could explain the high rate of heat storage gain in the morning and the high rate of heat storage loss in the late afternoon and early evening is found in section 6.

4.3. Mean Wind Fields in the Mexico Basin

During the winter dry season, the Mexico Basin is normally under the influence of anticyclonic weather with light winds above the basin and nearly cloudless skies, which is favorable for the development of thermally driven local and regional circulations.

Figures 7a-7d show mean daily wind soundings at the four basin sites, as composited from the low-range mode radar profiler wind data for the entire period of the field experiment except for the days of February 27 and 28 and March 1, 5, 6, and 13 when synoptic winds became unusually strong in the upper altitudes of the basin. The four figure parts are arranged so that the stations correspond to their relative geographical positions in the basin. The individual wind vectors in these plots are vector averages of all the 1-hour-average wind vectors at the indicated time and range gate for this period. The shading in the figure parts represents the day-to-day wind persistence, the ratio of the vector mean wind speed to scalar mean wind speed at the indicated range gates and hours over the period of record. If the wind always blows from the same direction, persistence is 1; if it is equally likely from all directions, or if it blows half the time from one direction and half the time from the opposite, it is zero. High values of persistence indicate that wind direction changes little from day to day, while low values indicate great day-to-day variability. The figure shows that the mean winds within the basin below a height of 1000-1500 m are extremely weak and variable in direction during much of the day (exceptions will be discussed in the following paragraph) and that diurnally reversing, low-level, along-valley winds, a key meteorological characteristic of valleys, are not readily apparent in the data. Another unusual characteristic of the Mexico Basin wind field is the tendency for the strongest winds within the basin to occur in the near-surface layer during the afternoon and evening as seen, for example, in the radar profiler wind data at Cuautitlan and Chalco (Figure 7). It was also noted in Doppler sodar data (which has range

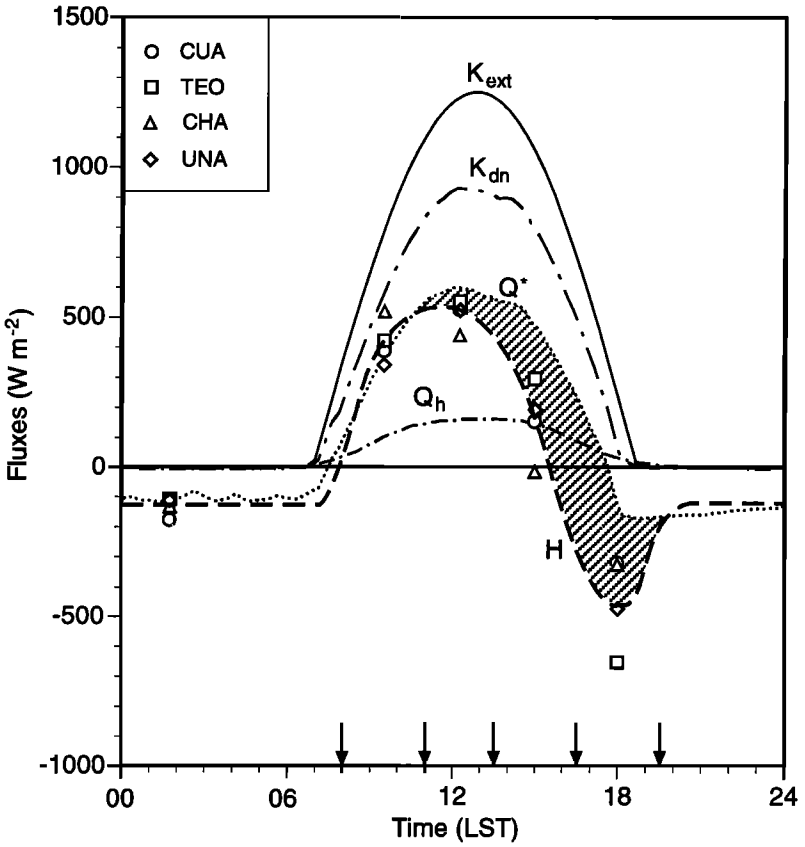

Figure 6. Instantaneous fluxes in the Mexico Basin as a function of time of day. The extraterrestrial solar flux (K_{ext}) is computed from a solar model; the incoming solar radiation (K_{dn}) and net radiation (Q*) were measured at UNAM on the clear day of March 1. Shown for comparison is *Oke et al.*'s [1992] 25-day composite sensible heat flux Q_h measurements obtained over the period from February 3 to March 31, 1985, in a heavily built-up part of Mexico City. The plotted data points indicated by symbols and fit by eye with a dashed line are mean rates of change of atmospheric heat storage (H) calculated from radiosondes using equation (1) for Cuautitlan (circles), Teotihuacan (squares), Chalco (triangles), and UNAM (diamonds). The data points are plotted at the midpoints between the sounding times. Sounding times are indicated by arrows. The hatched area emphasizes afternoon differences between the Q* and the H curves.

gates closer to the ground) and in rawinsonde data from the Mexico City Airport (not shown). The relatively high near-surface wind speeds may be attributed to the fact that the strongest afternoon horizontal pressure gradients between the basin and its cooler surroundings occur at the base of the deep CBL.

The highest day-to-day wind persistence (Figure 7) occurs at altitudes above 2800 m agl (about 5050 m msl) where southerly or southwesterly winds prevail above Cuautitlan, Teotihuacan, and UNAM and northerly or northwesterly winds prevail above Chalco. Weak southerly winds prevail above the basin in the residual layer (the elevated remnant of the daytime mixed layer) at all four basin sites usually beginning in late evening and lasting until sunrise. Some persistent winds also occur within the basin (i.e., below about 800-1000 m agl), but the characteristics of these winds differ from site to site. Above Cuautitlan, persistent northeast or north winds begin as early as 1000 LST. These weak winds increase in speed gradually after noon, gradually increase in depth to encompass the entire basin depth by midafternoon, strengthen significantly during the strong cooling period (1630 to 1930 LST), and then decrease in speed and depth until 0200 LST. The gradually increasing CBL depth above Cuautitlan is marked by a strong gradient in persistence at its top. At Teotihuacan a wind shift between weak afternoon westerly winds and stronger evening easterlies occurs during the rapid cooling period. Stronger easterlies come in at the end of the rapid cooling period and then decrease gradually in speed until midnight. At UNAM, winds are very weak during much of the day, except for northwesterlies that occur through the whole basin depth after 2200 and continue until 0200 LST. Winds during the rapid cooling period are weak and from the southwest. At Chalco a layer of strong, cool, south-southeasterly winds up to 1000 m deep enters the basin through the mountain gap to the southeast of the profiler site after 1300 and lasts until 2000 LST. The high persistence values associated with this flow indicates its day-to-day regularity. Low-level winds at Chalco are light during much of the remainder of the day.

Mean wind structure evolution in the Mexico Basin is consistent with the observed temperature structure evolution. At Chalco the strong south-southeasterly flow represents the

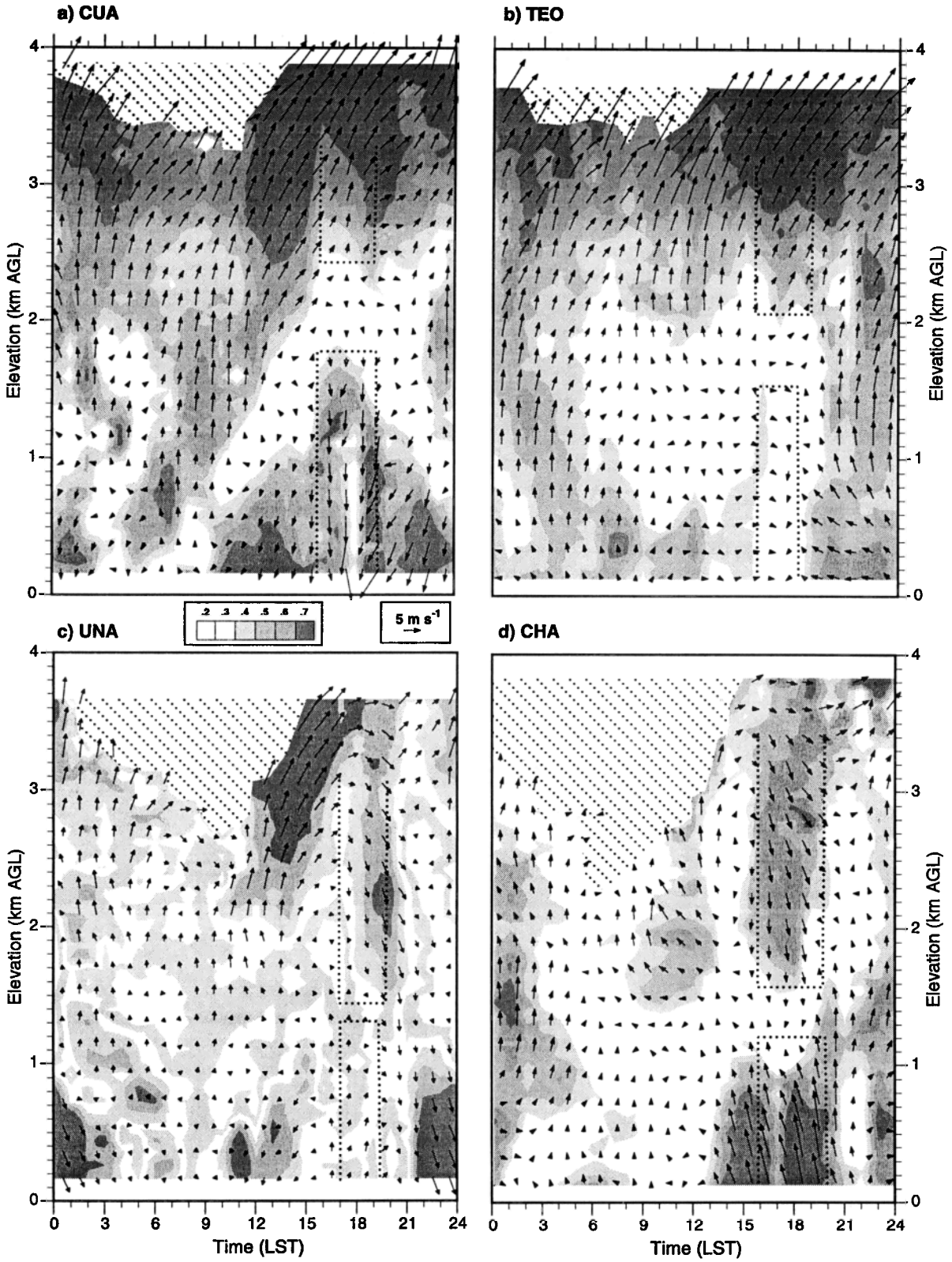

Figure 7. Mean daily vector wind patterns at (a) Cuautitlan, (b) Teotihuacan, (c) UNAM, and (d) Chalco. Persistence of the day-to-day winds is indicated with gray shades (see legend). Diagonal dotted lines indicate missing data. The dotted rectangles emphasize wind regimes at different levels of the atmosphere during the approximate times of the rapid cooling period. See text.

channeled advection of cool air into the basin through the mountain gap to the southeast of the basin. This cool air leakage starts, on the average, just after noon, and on some days even before noon, when the air inside the basin becomes warmer than the air outside, and it ends after the period of rapid cooling (1630-1930 LST) when the air temperatures within the basin begin to equilibrate with those of the surroundings (Figure 5). The leakage is probably responsible for the lack of heating of the boundary layer at Chalco between 1330 and 1630 LST as shown in Figure 2c and the slight stabilization of the temperature profiles within the convective boundary layer at Chalco relative to those at Teotihuacan (Figure 2a) and UNAM (Figure 2b). This gap flow occurred nearly every day during the 4-week experimental period regardless of the synoptic conditions, suggesting that it is driven by mesoscale pressure gradients produced by the overheating of the basin atmosphere relative to its surroundings. Further details on this gap wind system and its driving mechanisms have been discussed by *Zhong and Doran* [1998].

The northerly afternoon flow at Cuautitlan also represents cold-air advection or leakage into the warm basin. This advection is confined below the ridgetops, begins in the early afternoon when the basin becomes warmer than its surroundings, and is strongest near the ground where the horizontal potential temperature gradients (and horizontal pressure gradients) are strongest.

The basic characteristics of the cold-air intrusions are consistent with the diurnal evolution of temperature structure and heat storage in the Mexico Basin atmosphere. The cold-air leakage suppresses the heating and deepening of the basin boundary layer between 1330 and 1630 LST and causes the very pronounced afternoon falloff of the heat storage curve in Figure 6. The strengthening of cold-air advection in the evening, the convergence of the cold low-level flows over the basin floor and consequent rising motions above the convergence zone undoubtedly contributes to the rapid cooling above the basin between 1630 and 1930 LST. A low-level convergence and upper level divergence pattern is clearly seen in the profiler data of Figure 7 during the 1630 to 1930 LST period. These patterns are indicated by opposing wind directions between northern and southern parts of the basin and between lower and upper levels of the boundary layer (compare wind directions in the dashed-line boxes that correspond roughly to the rapid cooling period in Figure 7). A vertical advection explanation for the cooling of the basin atmosphere is appealing, because the horizontal flow strengths are not consistent between sites and are weak at both UNAM and Teotihuacan during the rapid cooling period, and because the cold-air advection is confined below the ridgetops, while the cooling extends above the ridgetops. Rising motions in a neutral atmosphere do not cause advective cooling, but as cooling occurs in the near-ground layer due to horizontal advection and downward sensible heat flux in the late afternoon and evening, rising motions caused by convergence can advect this cooling higher into the residual layer.

5. Model Simulations and Physical Mechanisms

The observations clearly point to a linkage between the regional wind circulations and the mesoscale temperature structure and heat storage of the Mexico Basin atmosphere. Although it is evident from the observations that these circulations are thermally driven, their exact nature is unclear. *Bossert* [1997] proposed that the northeasterly flow that influences the Mexico Basin during the late afternoon and evening is affected by several factors including the plain-to-plateau heating differential, the persistent surface high pressure over the Gulf of Mexico, and the sea breeze circulation along the coastal lowlands. He suggested that this large-scale northeasterly flow is similar to the mountain-plain circulation found along the Colorado Front Range [*Bossert and Cotton*, 1994a, b]. Further, he argued that although the mountain-plain circulation in the Front Range is a summertime phenomenon, the tropical latitude of central Mexico ensures sufficient insolation even in the wintertime to produce an analogous circulation between the lowlands and the high Mexican plateau. An alternate possibility is that the circulations in the Mexico Basin are more local in nature and develop in response to the overheating of the basin atmosphere relative to its immediate environs. In this scenario, air is drawn into the basin over the adjacent mountains by horizontal temperature differences that develop between the basin atmosphere and its surroundings. Although openings in the Mexico Basin make the topography somewhat different from the closed circular basin used in the simulations of *de Wekker et al.* [1998] and *Kimura and Kuwagata* [1993] and from the single-opening basin simulated by *Kimura and Kuwagata* [1993], such circulations would be similar to the idealized plain-to-basin flows studied by them. Note that in this case, the plain would be part of the elevated Mexican Plateau and not the coastal plain of *Bossert's* [1997] analysis.

Measurements of wind and temperature structure on the slope of the Mexican plateau which are needed to distinguish between these two possibilities are unavailable, so we turned to a numerical model to provide additional information. Specifically, we wished to extend *Bossert's* [1997] analysis to determine whether the coastal plain-to-plateau circulations simulated in that study were sufficient to explain the available observations or whether the features of the Mexico Basin significantly modified those circulations. We also wanted to make use of the much more extensive set of observations than was available to Bossert in his earlier study to examine some features of the Mexico Basin boundary layer.

The Regional Atmospheric Modeling System (RAMS) [*Pielke et al.*, 1992] was used for the model simulations. RAMS is a primitive equation, nonhydrostatic model based on a terrain-following coordinate system. Sub-grid-scale turbulent diffusion is parameterized using a level 2.5 scheme [*Mellor and Yamada*, 1982] with a prognostic turbulent kinetic energy equation and a diagnostic length scale. Turbulent sensible and latent heat fluxes and momentum fluxes in the surface layer are evaluated based on *Louis's* [1979] formulation. A multilayer soil model developed by *Tremback and Kessler* [1985] is used to predict diurnal variations in soil temperature and moisture. RAMS also contains a cloud microphysics package and a cumulus parameterization scheme, neither of which were activated for this study. Clouds, however, were allowed to form in areas of supersaturation on the basis of a diagnostic scheme, and the impact of clouds on radiation were included in the RAMS shortwave and longwave radiation schemes [*Chen and Cotton*, 1983].

Model simulations were carried out in two stages. In the

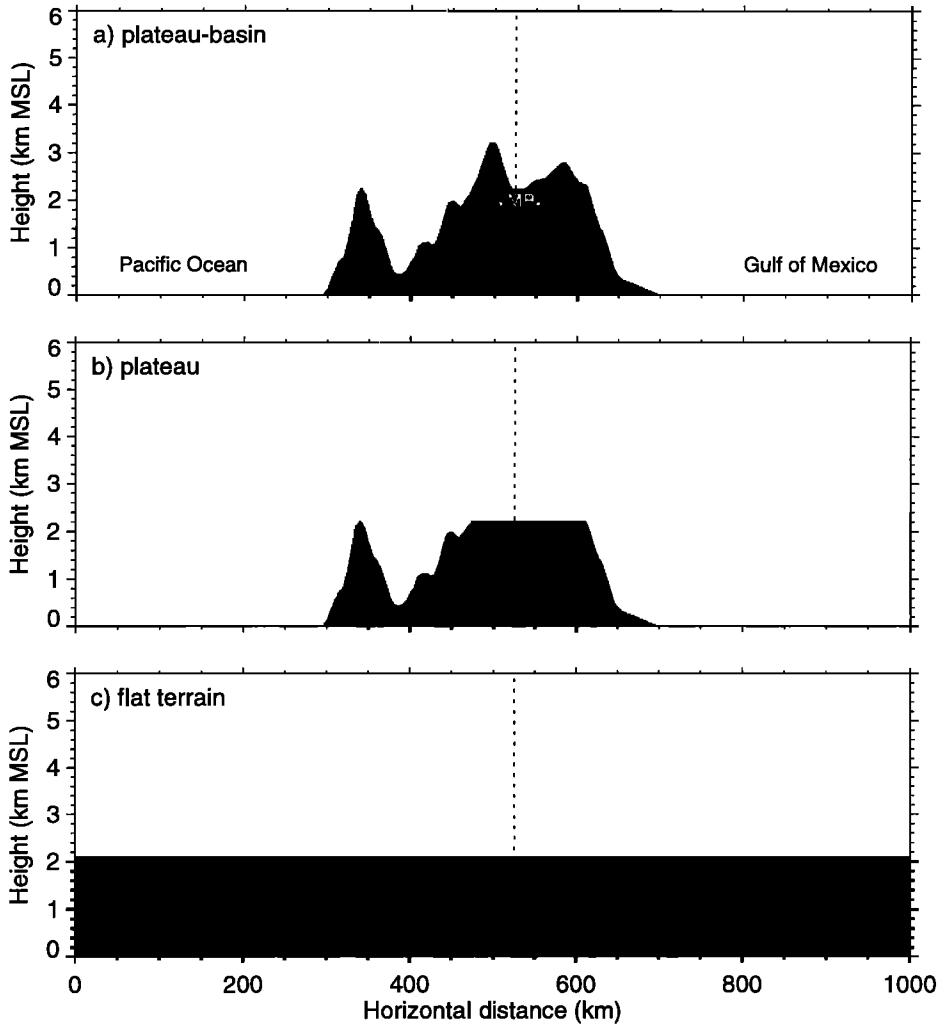

Figure 8. Terrain cross sections used in the (a) plateau-basin simulation (line A-A' in Figure 1), (b) plateau simulation, and (c) flat terrain simulation. The location of the Mexico Basin on the cross section is indicated by MB and arrows. Dashed vertical lines indicate the locations of temperature profiles in Figure 11.

first stage we used two-dimensional model simulations with several different terrain cross sections to investigate the nature of the circulations and the role of the terrain in their development. Three simulations were carried out. The first or plateau-basin simulation used a NE-SW vertical terrain cross section (Figure 8a) extending from the Pacific to the Atlantic Oceans across the isthmus and passing through the center of the Mexico Basin (line A-A' in Figure 1b). The second, or plateau simulation, modified the terrain cross section by eliminating the basin on top of the Mexican Plateau (Figure 8b). The third, or flat terrain simulation, used a flat homogeneous surface at the elevation of the Mexico Basin floor to provide a simulation of boundary layer evolution without modifications by plateau or basin topography (Figure 8c). In the second stage we used three-dimensional simulations in conjunction with the data from the 1997 measurement campaign to provide a more detailed picture of the flows in the Mexico Basin itself, to relate these flows to the heat budget in the basin, and to investigate the interaction and dependence of these flows on the larger-scale circulation patterns identified in the two-dimensional simulations.

5.1. Two-Dimensional Simulations

The modeling domain for the three two-dimensional simulations described above was 1000 km wide and 16 km deep. The horizontal grid spacing was 5 km and the vertical grid stretched from 20 m just above the surface to 1000 m at and above the 10-km level. A total of 60 vertical grid points were used with 35 of them in the lowest 4 km to resolve the boundary layer structure. This model configuration allowed good resolution of the terrain, including the Mexico Basin and the slopes of the Mexican plateau. A uniform soil type (sandy clay loam), vegetation type (semidesert), and soil moisture content were specified throughout the domain. A constant sea surface temperature, 295 K, was specified for the ocean areas. All simulations were initialized at 0600 LST with calm background winds using the mean temperature and moisture soundings from Acapulco (Figure 5). Simulations were run for 24 hours.

The simulated potential temperature and wind vector profiles at 1600, 1800, 2000, and 2200 LST are shown in Figure 9 for the plateau-basin simulation. At 1600 LST,

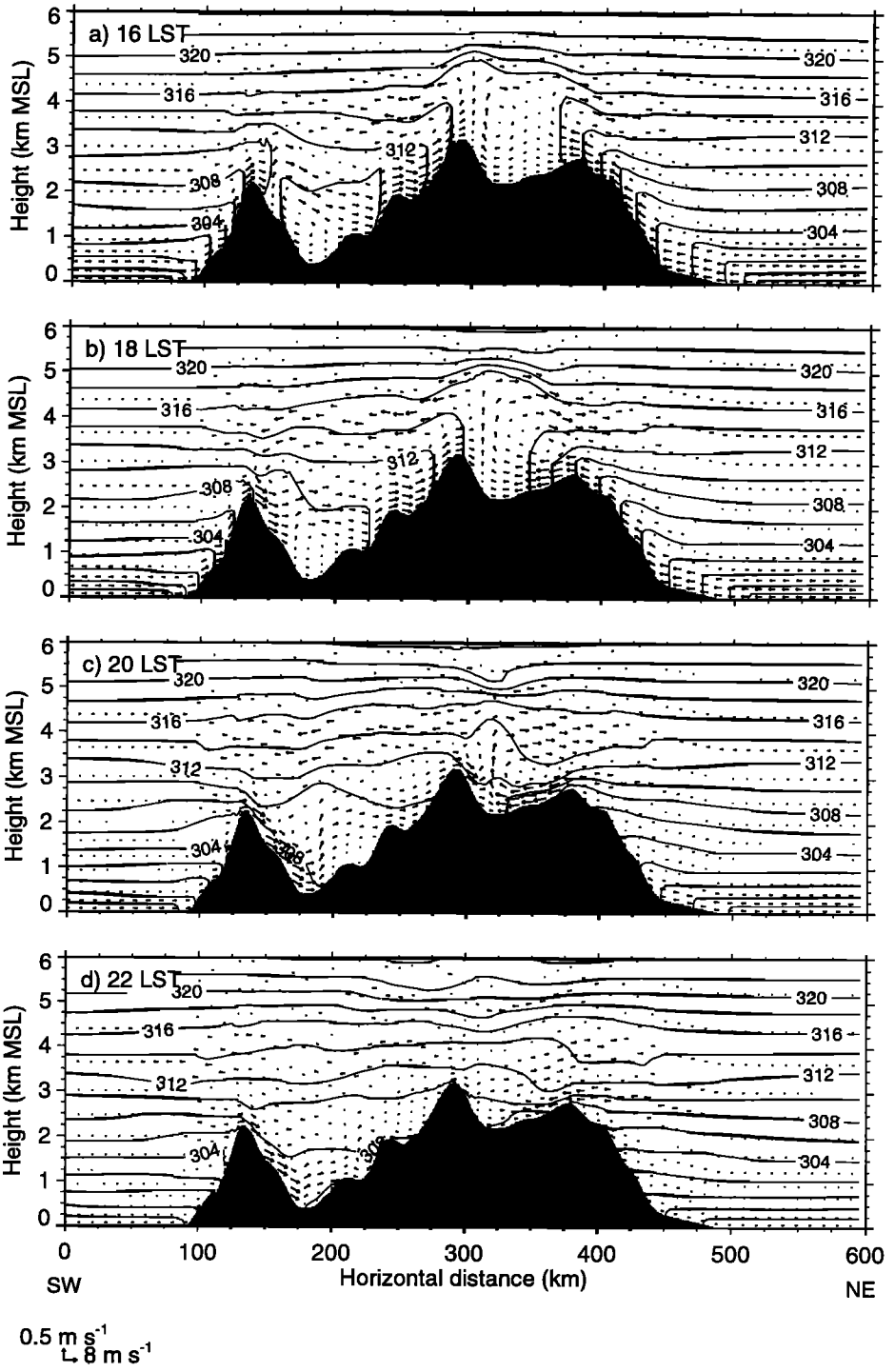

Figure 9. Isentropes and wind vectors for the two-dimensional, plateau-basin simulation at (a) 1600, (b) 1800, (c) 2000, and (d) 2200 LST. The topography (vertical cross-section A-A' in Figure 1) is indicated by the shading. The wind legend shows the different scales used for the horizontal and vertical wind components on this cross section.

boundary layer development over the top of the plateau and the plateau slopes differed considerably. A mixed layer deeper than 2 km developed over the plateau, and the boundary layer top was relatively uniform across the plateau, including the basin. The mixed layer over the slopes was much shallower than over the plateau. At the coast, onshore advection of cool marine air limited the mixed layer growth in conformance with radiosonde observations at the coastal sites (see Figure 5). A strong horizontal potential temperature gradient developed between the plateau/basin atmosphere and the atmosphere surrounding the plateau. The overheating of the basin atmosphere relative to its large-scale environment (see Figure 5) is therefore a result of the plateau topography acting as an elevated heat source during daytime. A deep

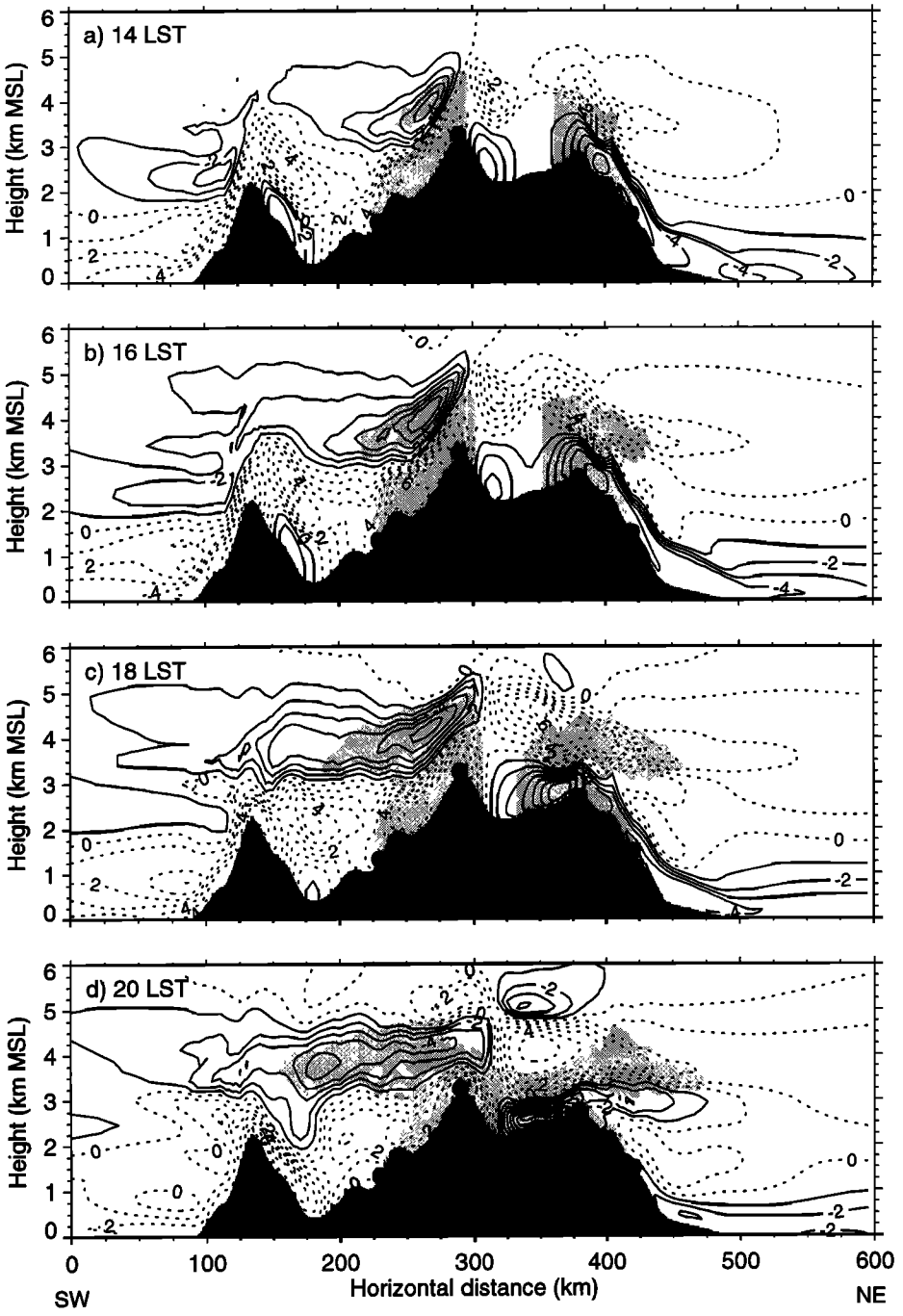

Figure 10. Particle plumes (light shading) and horizontal wind speed isopleths on the vertical cross-section A-A' (see Figure 1) at (a) 1400, (b) 1600, (c) 1800, and (d) 2000 LST. The dots indicate locations from which particles were released. Dashed isopleths indicate the speeds of horizontal winds blowing from left to right in the cross section; solid isopleths indicate wind speeds in the opposite direction. Contour interval is 1 m s^{-1}.

layer of upslope flow developed over slopes on both sides of the plateau, with weaker return flows aloft. The low branch of these plain-to-plateau circulations brings cooler, moister air from coastal regions to the top of the plateau along the slope surfaces, while the upper branch advects hotter, drier air away from the plateau. The circulations produce convergence at the edges of the plateau but have little impact on the basin at this time of the day. At 1800 LST the plain-to-plateau circulation penetrates farther into the interior of the plateau. The hot column over the plateau disappears between 1800 and 2000 LST after the plateau switches from an elevated heat source to an elevated heat sink near sunset and cold air flows rapidly to the foot of the mountains bordering the basin. The model simulations (Figure 9c) show that gravity waves are excited by the collapse of the dome at the top of the daytime convective boundary layer. These gravity waves propagate in

both directions when the heating of the boundary layer ceases, contributing to the rapid equilibration between the above-basin atmosphere and its surroundings over the next few hours, with isentropes becoming nearly horizontal. This equilibration accounts for the observed weak horizontal temperature gradients between the plateau atmosphere and its surroundings in morning rawinsonde soundings (see Figure 5a).

To help illustrate the behavior of thermally driven plain-to-plateau circulations and the differences in the depths of the mixed layer over the slopes and on top of the plateau, a Lagrangian particle dispersion model (LPDM) [*Fast*, 1995] was run using the mean wind and turbulence fields from the plateau-basin simulation. Nonbuoyant and nonreactive particles were released continuously from the surface at four sites in the domain shown in Figure 10: two on the edges of the plateau and two on the plateau slopes. The movements of the particles were tracked following their release. The rate of the release was 8 particles min^{-1} at each source and a total of over 30,000 particles were released during the course of the LPDM simulation, which commenced at 0600 LST in the morning and ended at midnight.

Figure 10 shows the simulated particle plumes along with the horizontal component of the winds on the cross section at 1400, 1600, 1800, and 2000 LST. At 1400 LST, after 8 hours of release, particles released over the slopes were mixed up to a 200- to 300-m-deep layer and were carried by the upslope flows along the slope surface to the edges of the plateau; there, they were further mixed vertically, along with those released from the plateau edges, to a much deeper layer. Two particle fronts (the leading edges of the particle plumes) were clearly defined at this time: one on the ridgetop on the left and one a short distance onto the plateau from the plateau edge on the right. The particle fronts tended to remain anchored over the mountains at the edges of the plateau throughout the morning and early afternoon by upslope flow convergence and intense rising motions over the mountaintops. Well-defined return flow layers advected particles that were mixed to higher elevations back toward the coastal regions. In late afternoon and evening (1600 and 1800 LST) when CBL heating slowed and reversed to cooling, particle fronts accelerated onto the plateau as air flowed across a baroclinic zone that had developed during daytime on the periphery of the plateau and separated the warm plateau CBL from its cooler surroundings. By 2000 LST the two fronts moving onto the plateau merged over the basin, and particles filled the atmosphere over the plateau and basin to a height well above the ridgetop.

The simulated potential temperature profiles from the three simulations for 0800, 1100, 1400, 1700, and 2000 LST are shown in Figure 11. The profiles are taken from the grid point near the center of the basin on the terrain cross section for the plateau-basin simulation (Figure 8a) and from the same grid point for the two other simulations. Both the plateau-basin and the plateau simulations produce a daytime boundary layer that evolves in a fashion similar to the observed pattern (Figures 11a and 11b), with rapid growth between 1100 and 1400, which slowed between 1400 and 1700, and rapid and deep cooling between 1700 and 2000 LST. In the flat terrain simulation (Figure 11c), however, significantly different boundary layer behavior is produced in late afternoon; there, very little cooling occurs between 1700 and 2000 LST, and the cooling is largely confined near the surface. The CBL height in the afternoon in the flat terrain simulation is also lower than for the other two simulations. A closer comparison between the profiles from the plateau-basin simulation and those from the plateau simulation indicates that somewhat more heating during the day and more cooling in the evening hours occurred in the plateau-basin simulation. This behavior is consistent with the TAF (Topographic Amplification Factor) concept which states that heating and cooling are likely to be amplified in a basin or valley environment by the terrain [*Whiteman*, 1990]. Nonetheless, the most pronounced characteristic of boundary layer development in the Mexico Basin, namely, the rapid evening cooling that extends through the entire afternoon boundary layer, is determined primarily by the plateau topography rather than the basin topography.

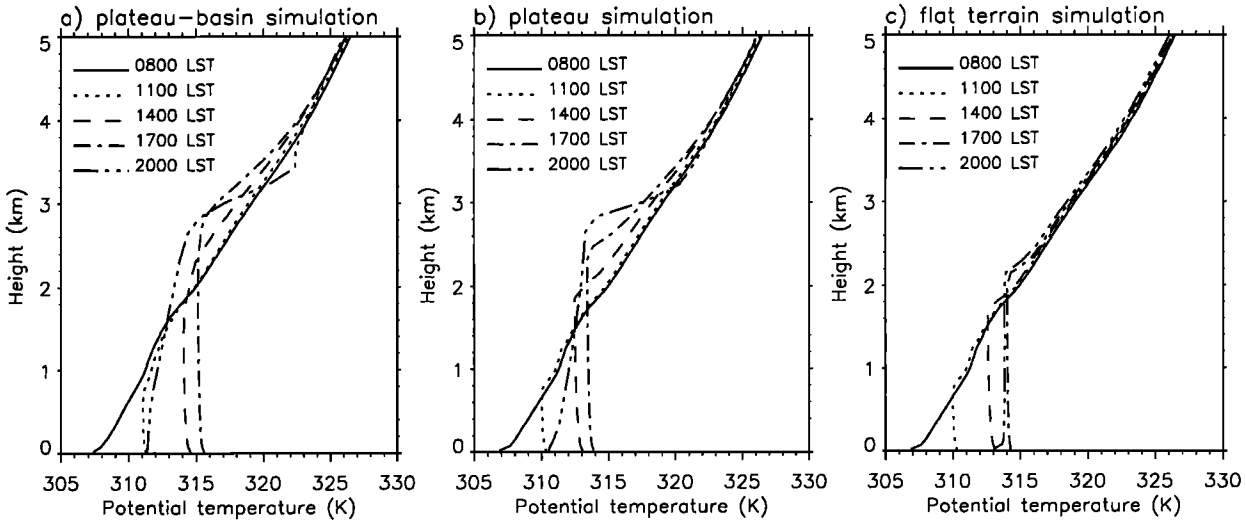

Figure 11. Potential temperature profiles at 0800, 1100, 1400, 1700, and 2000 LST from (a) plateau-basin simulation, (b) plateau simulation, and (c) flat terrain simulation. The location of the profiles was shown by the dashed line in Figure 8.

5.2. Three-Dimensional Simulations

To provide additional insight on how the plain-to-plateau circulations affect the boundary layer characteristics inside the Mexico Basin, several cases chosen from the field experiment were simulated using a three-dimensional model configuration. Results from a 2-day period (0600 LST on March 3 to 0600 LST on March 5) are presented here. The four radar wind profilers indicated predominately north-northeasterly winds above ridgetops at moderate speeds during this time period. Inside the basin, winds were generally weak during the morning hours on each day and became much stronger in late afternoon and evening as thermally driven flows entered the basin The modeling domain consisted of three nested grids at horizontal resolutions of 36, 9, and 2.25 km, respectively. The innermost grid covered the Mexico Basin area, while the outer grid encompassed the entire isthmus and the surrounding ocean surfaces (Figure 1). All three grids had 42 vertical levels, stretched from a grid spacing of 50 m near the surface to 1500 m at the model top at 17.8 km. Twenty-six vertical nodes were placed in the lowest 4 km to allow a detailed description of the observed deep boundary layer development over the basin. Eleven soil nodes were used to a depth of 1 m below the ground surface. Soil type was specified as sandy clay loam throughout the domain. The initial soil moisture content was set to 20% of the saturation value for all 11 soil layers across the domain to reflect the dry wintertime conditions. Vegetation cover in the domain was specified from a U.S. Geological Survey 1 km database (159 categories) which was converted to 18 BATS (Biosphere - Atmosphere Transfer Scheme [*Dickinson et al.*, 1986] categories in RAMS. Emissivity, albedo, and roughness length values were set to 0.95, 0.15 , and 2 m, respectively, for the Mexico City metropolitan area. Surface temperatures at the ocean grid points were determined by interpolation from 2-week composite sea surface temperature analyses at 1° horizontal resolution. The model was initialized at 0600 LST on March 3 with objective analysis fields determined from the National Centers for Environmental Prediction (NCEP) aviation model and assimilation of standard U.S. and Mexico rawinsonde soundings. The five outermost lateral boundary points in the largest domain and the top boundary points on all three grids were nudged using a simplified Davies scheme [*Wang and Warner*, 1988] toward the objective analysis fields to allow changes in large-scale conditions to influence the model simulations. Hourly wind profiles at the four basin sites were also assimilated during the simulations.

To help understand the mechanisms responsible for the evolution of the temperature profiles, we examined the modeled heat budget for the basin, which can be written as

$$c_p \int_0^{1\,\mathrm{km}} \overline{\rho \frac{\partial \theta}{\partial t}} dz = c_p \int_0^{1\,\mathrm{km}} \overline{\rho \{ \underbrace{-\left(u \frac{\partial \theta}{\partial x} + v \frac{\partial \theta}{\partial y}\right)}_{\mathrm{I}} \underbrace{- w \frac{\partial \theta}{\partial z}}_{\mathrm{II}} + \underbrace{\frac{\partial}{\partial z}\left(K_z \frac{\partial \theta}{\partial z}\right)}_{\mathrm{III}} + \underbrace{\frac{\partial F_N}{\partial z}}_{\mathrm{IV}} \} dz} \quad (2)$$

where the overbar indicates a horizontal average over a rectangular area on the basin floor bounded approximately by the four profiler sites (Figure 1a). Equation (2) was obtained by horizontally averaging and vertically integrating the thermodynamic energy equation, which states that the change of heat storage in the air column above the basin floor is produced by horizontal advection (I), vertical advection (II), turbulent flux convergence (III), and radiative flux convergence (IV).

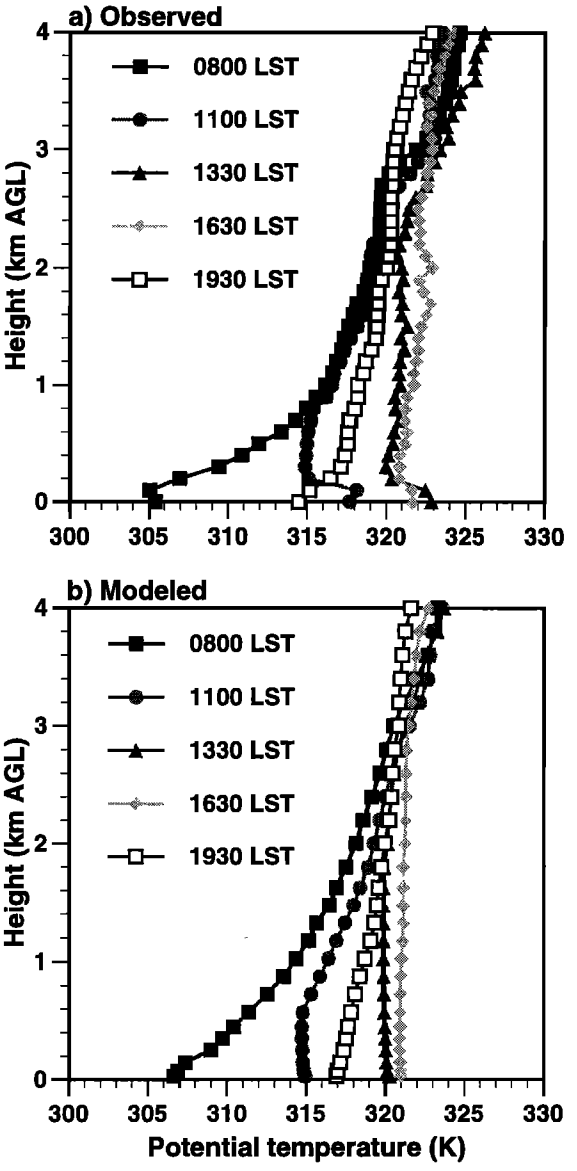

Figure 12. (a) Observed and (b) simulated potential temperature profiles on March 4, 1997. The observed profiles are averaged over the four basin sites Teotihuacan, Cuautitlan, UNAM, and Chalco, while the simulated profiles are averaged from the grid points closest to the four sites.

Before examining the individual terms in the heat budget it is important to consider possible sources of error in their evaluation. We have no independent means of estimating the sensible and latent heat fluxes over the Mexico Basin, nor do we have soil moisture measurements that could be used to initialize the surface energy budget module in the model. Similarly, there are no measurements of aerosol or trace gas concentrations that can be used to estimate the magnitude of possible contributions from radiative flux divergence.

Despite such uncertainties, the model does a credible job in simulating many of the important features of the boundary layer structure and evolution in the Mexico Basin. A com-

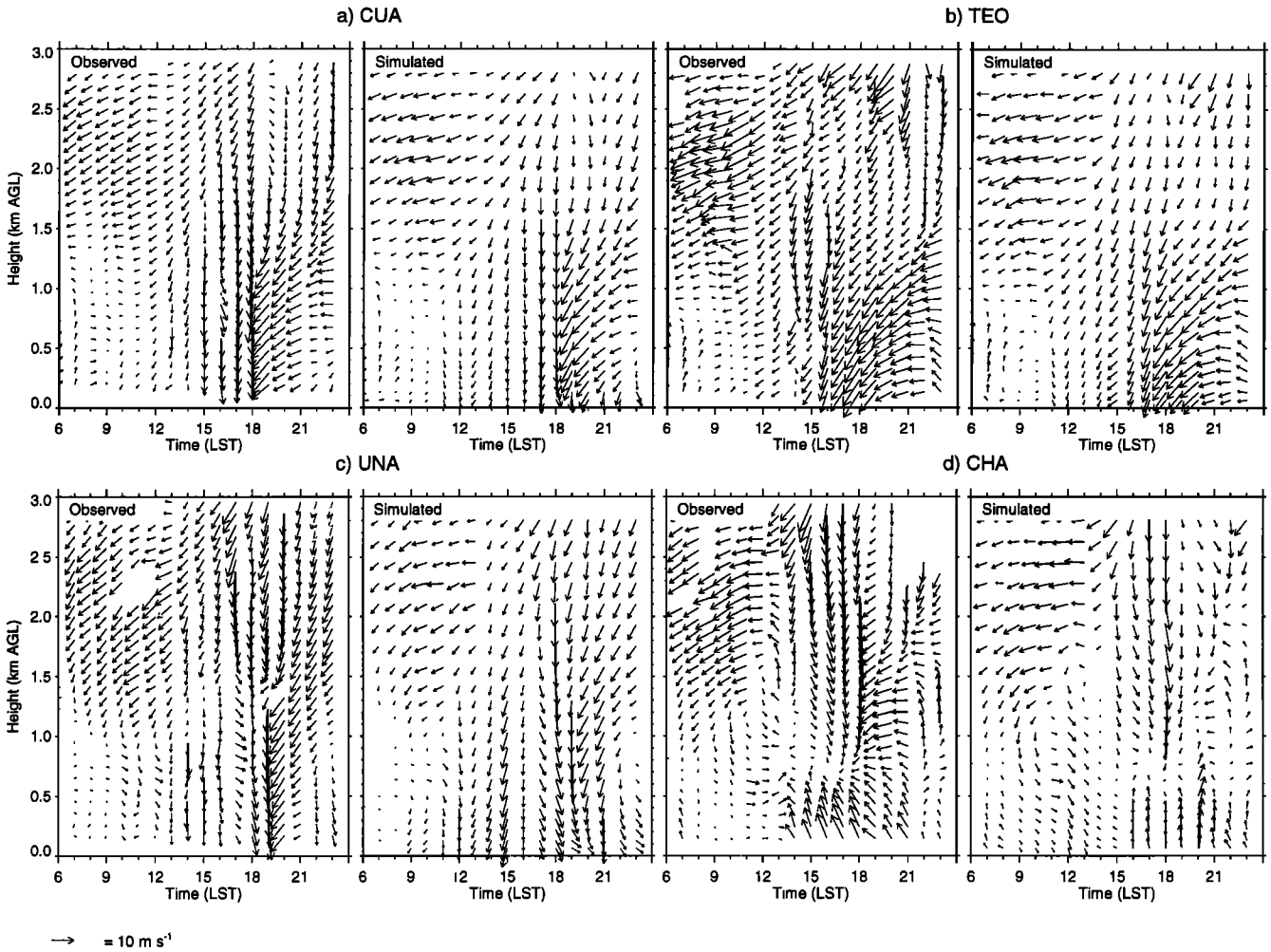

Figure 13. Simulated and observed hourly horizontal wind vector profiles on March 4, 1997, at (a) Cuautitlan, (b) Teotihuacan, (c) UNAM, and (d) Chalco.

parison of observed and simulated potential temperature profile evolution on March 4, the second day of the simulation, is shown in Figure 12. The observed profiles are averages over the four rawinsonde sites inside the basin and thus represent the temperature evolution of the entire basin atmosphere. The simulated profiles are averages of the profiles at the four grid points nearest to the four observation sites. The basin atmosphere on this day exhibited the three typical stages of boundary layer evolution inside the basin, i.e., rapid warming and growth between 1100 and 1330 LST, a much slower growth between 1330 and 1630 LST, and rapid cooling through a deep layer between 1630 and 1930 LST. The three stages in boundary layer evolution were captured by the simulation reasonably well, but the modeled CBL heights were slightly lower and the temperatures within the CBL were 1-2 K lower than observed in the afternoon. The simulated total cooling in the evening was also lower. A comparison of simulated winds with the profiler measurements shows reasonably good agreement at all four sites (Figure 13). The biggest differences between the observations and the simulations are at UNAM, where the sudden shift in wind direction after 1900 LST is not well resolved, and at Chalco, where simulated afternoon and evening low-level winds are too weak, and simulated early evening winds in the elevation range from 0.5 to 2 km do not agree well with observations.

Turning to the heat budget analysis, Figure 14 shows a time series of the individual terms of equation (2). As expected, through most of the morning and early afternoon, turbulent flux convergence heats the basin atmosphere, while horizontal advection cools the basin atmosphere. The heat storage peaks around noon as the turbulent flux convergence reaches its maximum and decreases rapidly in the afternoon with decreasing turbulent flux convergence and increasing cold-air advection. The switch from heat gain to heat loss occurs around sunset when the heat storage term changes sign, and the rapid heat loss during the next several hours is dominated by horizontal cold-air advection. This behavior is consistent with the observations. After the period of rapid cooling, the horizontal cold-air advection becomes relatively small and eventually changes from cooling to warming in the late night and early morning when the basin atmosphere becomes colder than the surrounding air. The nighttime cooling of the air within the basin is produced by turbulent and radiative flux divergence, which is partly compensated by vertical advection.

The role of advection in the rapid cooling of the basin

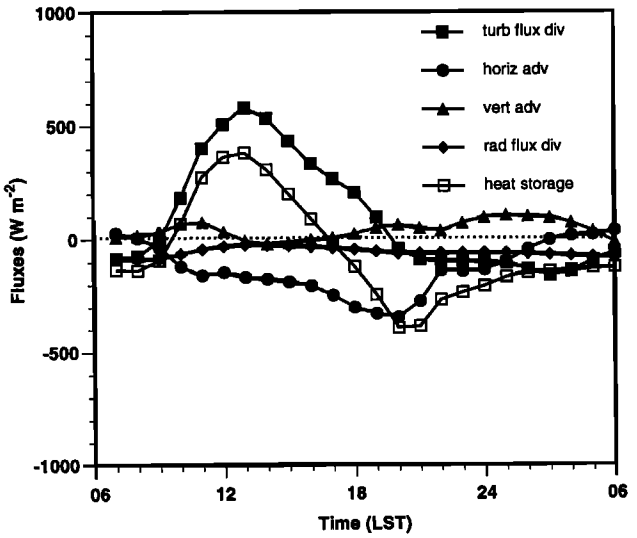

Figure 14. Diurnal variation of the individual terms of the model heat budget equation (equation (2)) as averaged horizontally over the basin floor and integrated vertically to 1 km above the ground.

atmosphere in late afternoon and evening can also be seen in Figure 15, which shows vertical profiles of the model temperature tendencies averaged between 1600 and 2000 LST. As seen from the heat storage curve, the cooling occurs throughout the entire boundary layer, with the rate of cooling decreasing from approximately 2 K h^{-1} near the basin floor to about 1 K h^{-1} at 2 km. The cooling is dominated by horizontal advection below 1600 m and by vertical advection above 1600 m.

As noted above, the heat loss derived from the temperature soundings between 1630 and 1930 LST was larger than the simulated loss, so the heat budget terms illustrated in Figure 14 for this period could not account fully for the observations. The smaller simulated heat loss in the evening was mostly the result of lower than observed afternoon temperatures in the simulation, suggesting that either the simulated cold-air advection was too strong or the sensible heat flux was too small in the afternoon. In other cases that we simulated, the model often predicts moderate to strong southerly downslope flows at the UNAM site late in the afternoon. The profiler at UNAM, however, observes weak southerly or northerly flows during these times. This discrepancy results in a further uncertainty in the heat budget terms. At this time therefore we must conclude that the model is not able to provide a sufficiently detailed representation of the boundary layer structure and dynamics to fully explain the observed heating and cooling rates shown in Figure 6. Nevertheless, it does appear to give a qualitatively reasonable description of the roles of the most important contributions to the heat budget and it also provides useful information on the interaction of the basin and plateau winds. We turn our attention to some of these features next.

The simulated horizontal wind fields at 250 m agl in the afternoon and evening in the area of the basin (grid 3) and over the plateau (grid 2) are shown in Figure 16. Early in the afternoon at 1400 LST, strong easterly to northeasterly flows developed over the slopes to the northeast which separate the elevated Mexico plateau from the coastal plains along the Gulf of Mexico (Figure 16a). These flows were a prominent feature in the *Bossert* [1997] simulations. An observational study by *Fitzjarrald* [1986] found similar flows in the Veracruz region (Figure 1). The simulation shows that the strong winds were mainly found over the slopes, while wind speeds on top of the plateau were much smaller. Upslope flows also developed over the slopes of the mountains surrounding the basin to the south, southeast and southwest. These upslope flows were again limited to the slopes and had little impact on the basin except near the gap in the mountains to the south-southeast, where a strong southerly flow started to enter the basin just after this time (Figure 16c). The wind through the gap and the general upslope flow from the north-northeast brought cooler air into the heated basin in early afternoon, slowing down the rate of heating of the basin atmosphere. By 1800 LST the strong northeasterly flow that originated over the northeast slope of the Mexico plateau prevailed over the northeast part of the plateau and had entered the basin through the open northern end (Figures 16b and 16d). Southerly winds through the gap also intensified. The convergence of the northerly and southerly winds within the basin led to the generation of a strong convergence zone in the southern part of the basin (Figure 16d).

These results from the three-dimensional (3-D) model simulation illustrate how the inflow of cooler air through the openings to the basin reduced the afternoon heating rate, and they suggest that horizontal cold-air advection was the major cause for the early-evening rapid cooling of the atmosphere in the basin, and rising motions associated with low-level convergence were mostly responsible for the cooling above the basin. The results also suggest that the cold-air advection is a result of plain-to-plateau circulations that bring air up the slopes along the Gulf coast to the northeast and the slopes of the mountains that form the southern boundary of the basin. These plain-to-plateau circulation systems, first investigated

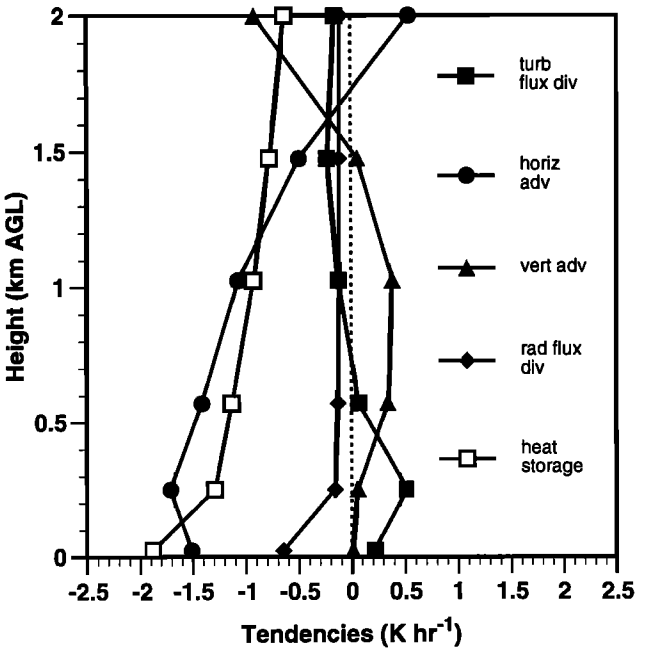

Figure 15. Vertical distribution of individual terms of the model heat budget equation as averaged horizontally over the basin floor and temporally between 1600 and 2000 LST.

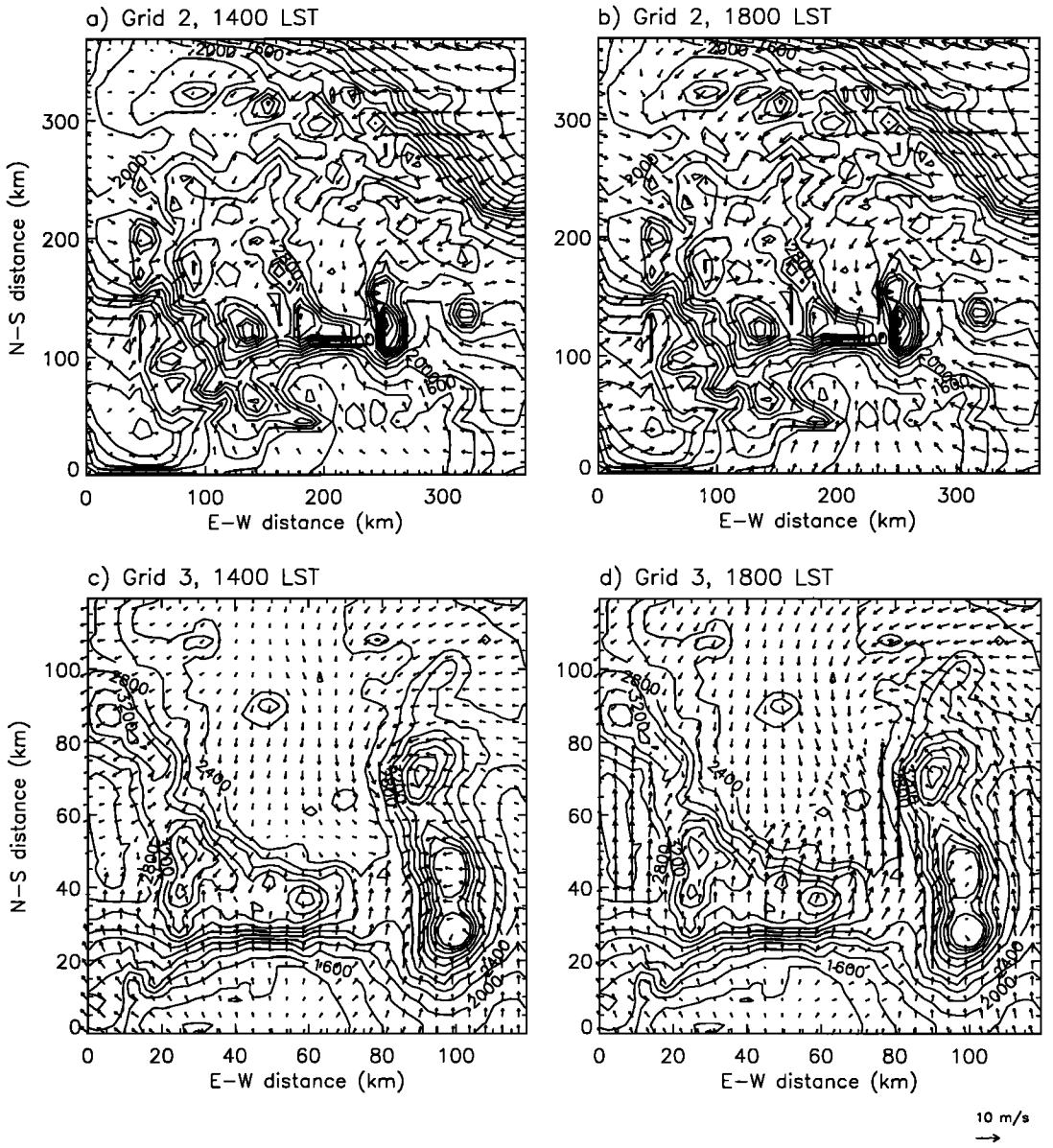

Figure 16. Simulated horizontal vector wind fields (arrows) at 250 m agl on March 4 on grid 3 at (a) 1400 and (b) 1800 LST and on grid 2 at (c) 1400 and (d) 1800 LST. Contours are terrain heights at 200 m intervals. The wind legend applies to all four figure parts.

by *Bossert* [1997], appear to occur regularly, as is evident from the composite observed wind profiles in Figure 7, and they were simulated well in all the cases studied. The strength of these circulations and their influence on the development of the boundary layer over the Mexico Basin varied from day to day, depending on synoptic wind speed and direction.

The simulations show that the cool, moist air that flows rather suddenly onto the plateau in the late afternoon or early evening is not a sea breeze front that advances up the outer slopes of the plateau and breaks onto the plateau at this time. No such traveling front is apparent in the simulations. Furthermore, sea breeze fronts would have different arrival times every day, depending on the speed of the advancing front and the distance to the coast, which would vary with synoptic wind directions and position in the basin and would not be consistent with the rather regular time of the cool-air arrival on the plateau. The simulations, rather, show that the cool, moist air from the coastal areas is advected up the outer slopes of the plateau in a plain-plateau circulation, moistening and cooling the air surrounding the plateau and forming a baroclinic zone on the plateau edges. In the afternoon a flow begins to form across the baroclinic zone onto the plateau but is held back in locations where mountains or steep slopes on the plateau edges anchor the rising branch of the plain-plateau circulation. The flow accelerates onto the plateau in the late afternoon, however, when the energy budget reverses on the plateau and the plateau CBL starts to decay. At this time, the energy budget has also reversed on the slopes, ending the upslope flows on the plateau outer slopes. Thus the air flowing onto the plateau does not represent a continuous flow up the slopes from the coastal areas. Rather, air flowing onto the

plateau comes from the air mass surrounding the plateau that has been moistened during the day by the plain-plateau circulation.

6. Discussion of Energetics

The energetics calculations in section 5.2 showed that the rate of gain of heat storage in the boundary layer between sunrise and noon was much higher than expected from estimates of surface sensible heat flux. Further, the rate of decrease of heat storage in the late afternoon and early evening could be explained only by cold-air advection (both horizontal and vertical), and the nighttime rate of loss of heat storage was in excess of what could be expected from sensible heat flux alone. Processes that could explain the enhanced cooling or warming fall into several categories: turbulent sensible heat flux divergence, potential temperature flux associated with the mean wind (i.e., advection), and radiative flux divergence. These processes are discussed, in turn, below.

No sensible heat flux measurements were available from the IMADA-AVER experiment for comparison to the atmospheric heat storage calculations. Measurements by *Oke et al.* [1992] during a similar time period (February 3 through March 31, 1985) were made in a heavily built-up section of Mexico City (Tacubaya) where the sensible heat flux was greatly reduced during daytime by the storage of heat in dense building materials and did not become negative at night because of heat release from storage (see Figure 6). Oke et al.'s 25-day-average flux curve was sinusoidal with the peak flux reaching only 165 W m^{-2} at midday. T. R. Oke (personal communication, 1998) has suggested that sensible heat flux in the rural areas of the basin during daytime might reach as high as 80% of the net radiation. Figure 6 shows, however, that 100% of the measured net radiation gain at the surface during daytime and net radiation loss during nighttime would have to be converted to sensible heat flux to explain the observed heating or cooling of the atmosphere, if one assumes that the heat sources and sinks are localized within the basin and that surface sensible heat fluxes are the sole cause. Because the surface energy budget is driven by net radiation gain or loss, and some of this energy will be partitioned into ground heat flux and latent heat flux, some of it will be unavailable for heating or cooling the atmosphere. The entrainment flux at the top of a growing CBL, typically adding approximately 20% of the surface sensible heat flux [*Stull*, 1988], cannot be the source of the missing energy because the energetics calculations are made through depths well above the CBL where the downward turbulent sensible heat fluxes are expected to be negligible. Two processes have been proposed previously which are capable of amplifying the sensible heat flux in complex terrain areas relative to observed sensible heat fluxes on the basin floor or observed fluxes in flat terrain areas. First, sensible heat fluxes on mountain slopes are expected to be higher than measured fluxes on a basin floor because of the shear and turbulence associated with upslope flows [*Whiteman et al.*, 1996, *Fast et al.*, 1996]. Thus measurements on the floor of a basin are not representative of the basin as a whole. Second, in an enclosed volume such as that in a basin or valley, energy inputs and outputs produce larger air temperature increases and decreases than would be produced in a flat-floored volume of the same depth and drainage area [*Steinacker* 1984]. The amplification of the daily temperature range in a confined topographic volume relative to a volume that is not limited by the sloping sidewalls, termed the topographic amplification factor (TAF), can reach 2 in linear v-shaped valleys and 3 in axially symmetric basins with v-shaped cross sections [*Whiteman*, 1990]. However, the broad Mexico Basin, with a nearly flat floor, would have an amplification only fractionally larger than 1, and its effective TAF would be reduced further toward 1 after the daytime CBL grows above the height of the ridgetops, as heat would no longer be confined within the basin.

Because the air in the coastal areas surrounding the plateau and basin is considerably cooler than the air over the basin during daytime and only slightly warmer by sunrise (Figures 5b and 5a), advection on this scale is incapable of producing daytime warm air advection over the basin, except during a brief period after sunrise, and cannot explain the enhanced daytime atmospheric heat storage rates, which exceed what would be obtained with a sinusoidal surface sensible heat flux curve that peaks at 600 W m^{-2} at noon (Figures 3 and 6). On the basin scale, however, upslope flows, which form over the basin inner sidewalls after sunrise, with warm rising air over the heated slopes and compensatory sinking motions producing warming over the basin center, are likely to produce enhanced heating in the basin during the first few hours after sunrise. Similarly, convergence of downslope flows over the basin center at night with corresponding rising and cooling over the basin center are likely to enhance the nighttime cooling.

Radiative flux convergences or divergences might help to explain the enhanced warming and cooling rates in the basin. Absorption of solar radiation by boundary layer aerosols has been proposed by earlier investigators [e.g., *Zdunkowski et al.*, 1976; *Ackerman*, 1977] to explain enhanced warming in polluted atmospheres. *Angevine et al.* [1998] recently estimated that direct aerosol heating accounted for 20% of the total heat flux from all sources in a case study of boundary layer growth near Champaign-Urbana, Illinois. Direct radiative absorption by aerosols heats the boundary layer without the losses to latent heat flux and ground heating that would occur if this conversion of solar radiation to sensible heat flux occurred at the ground. If direct solar absorption occurs on aerosols, insolation at the surface would decrease. This feature could be tested in the future with a line of pyranometers up one of the slopes above Mexico City.

7. Conclusions

Data analyses and numerical model simulations have been used to investigate the evolution of boundary layers and diurnal wind systems over the Mexico Basin and Mexican plateau during the winter dry season and to determine how the topography affects this evolution.

The Mexico Basin, where Mexico City is located, exhibits few of the meteorological characteristics of a basin or valley. It does not have a well-developed diurnally reversing valley wind system as one would expect from a valley, and it does not develop the strong nighttime temperature inversions expected of a basin. Rather, the main meteorological features seen in analyses and simulations are associated with the Mexican plateau on which the basin is located. A deep mixed layer grows above the isolated plateau during daytime, producing a strong horizontal temperature contrast between the warm air over the plateau and the cooler air in the surroundings of the plateau. Regional diurnal wind systems are driven

by the strong thermal contrasts, bringing cool air from the surrounding ocean areas onto the plateau during daytime and strongly affecting the diurnal evolution of the boundary layer over the plateau. The phasing of these diurnal circulations is especially interesting.

The rate of change of atmospheric heat storage in the air column above the basin was calculated from the heating or cooling observed between consecutive potential temperature soundings. The rate of change of heat storage exhibits a temporal asymmetry relative to solar noon. The atmospheric heat storage increases rapidly in the morning but falls off gradually after noon. Simulations attribute the afternoon falloff in the rate of increase of heat storage to regional diurnal winds that bring cool air onto the plateau and through gaps into the basin, suppressing the afternoon CBL development somewhat. This afternoon leakage of cold air onto the plateau from the surroundings occurs preferentially on low edges of the plateau. Where mountains are present at the plateau edges or the edges of the plateau are steep, the terrain effectively holds back the afternoon flow of air onto the plateau by virtue of strong rising motions that form over the plateau edges. These rising motions represent the rising branch of a plain-to-plateau circulation that forms over the coastal plains and plateau slopes with a return flow aloft toward the coastal areas and sinking motions over the oceans. This circulation produces an intense baroclinic zone around the periphery of the plateau during daytime, separating the warm air in the convective boundary layer over the plateau from the cooler air surrounding the plateau.

The surface energy budget on the plateau and its side slopes reverses shortly before sunset. At this time, the strong rising motions that anchor the plain-to-mountain circulations on the plateau edges cease and cool air converges onto the warm plateau rather suddenly as air flows across the baroclinic zone that has built up during the day around the periphery of the plateau. The regional-scale flow onto the plateau is strongest at the lowest levels of the atmosphere where the horizontal temperature gradients are strongest. The horizontal convergence of cool air onto the plateau and into the basin leads to rising motions that rapidly cool the atmosphere above the plateau and basin. Observations above the basin document this very rapid cooling which, between 1630 and 1930 LST, counteracts more than half of the daytime heat storage gain. Equilibration between the warm boundary layer air over the plateau and the cooler air surrounding the plateau is enhanced not only by the increased cold air inflows at low levels but also by gravity waves that propagate away from the plateau center when the domed entrainment zone (Figures 9a and 9b) at the top of the daytime convective boundary layer dissipates (Figures 9c and 9d). The equilibration produces horizontal isentropes across the Mexico isthmus by late night, so by sunrise, the temperature and stability of air over the plateau differ little from air surrounding the plateau at the same elevation. The surface energy budget reversal that signals the sudden increase of regional scale convergence also produces shallow downslope flows over the inner and outer slopes of the plateau. Local downslope flows that develop on the inner sidewalls of the basin add to the regional convergence. These flows continue through the night after the regional-scale flows decay, producing a marginally enhanced stable layer above the floor of the Mexico Basin as cold air converges over the basin floor.

Our research follows *Bossert*'s [1997] meteorological case study simulations of the Mexico Basin and has confirmed several aspects of his work, including his basic finding that regional and multiscale flows have important effects on the Mexico City area (and thus on air pollution dispersion). We have added further information on boundary layer development, energetics, and climatology. Our simulations make use of the same mesoscale meteorological model, and while having access to larger quantities of experimental data, we must reiterate his comments regarding the lack of experimental data against which to evaluate the model simulations, especially those on the plateau scale beyond the boundaries of Mexico City. Further data are needed on the wind and temperature structure evolution above the slopes of the basin and the plateau and on the surface and atmospheric energy budgets over the region. The role of Mexico City aerosols on the atmospheric heat budget, the role of gravity waves in the destruction of the daytime mixed layer, and the origin, structure, and timing of air currents coming onto the plateau and into the Mexico Basin are all topics that need further work. Our model-based diagnostic studies have pointed out several areas where model improvements are needed for complex terrain simulations.

Acknowledgments. We thank the IMADA-AVER field study participants for use of their data. We thank our colleagues at Pacific Northwest National Laboratory (PNNL) for useful discussions (J. M. Hubbe and W. J. Shaw) and for valuable reviews of our manuscript (W. R. Barchet). This research was supported by the U.S. Department of Energy, Office of Biological and Environmental Research, Environmental Sciences Division as part of their Atmospheric Studies in Complex Terrain program under contract DE-AC06-76RLO 1830 at PNNL. The U.S. Department of Energy PNNL is operated by Battelle Memorial Institute.

References

Ackerman, T. P., A model of the effect of aerosols on urban climates with particular applications to the Los Angeles Basin, *J. Atmos. Sci.*, *34*, 531-547, 1977.

Angevine, W. M., A. W. Grimsdell, S. A. McKeen, and J. M. Warnock, Entrainment results from the Flatland boundary layer experiments, *J. Geophys. Res.*, *103*, 13,689-13,701, 1998.

Bian, X., C. D. Whiteman, G. S. Iglesias, and E. W. Garcia, Climatological analyses of air pollution in the Mexico Basin, in *Preprints, 10th Joint Conference on Applications of Air Pollution Meteorology with the Air and Waste Management Association*, pp. 382-386, Am. Meteorol. Soc., Boston, Mass., 1998.

Bossert, J. E., An investigation of flow regimes affecting the Mexico City region, *J. Appl. Meteorol.*, *36*, 119-140, 1997.

Bossert, J. E., and W. R. Cotton, Regional-scale flows in mountainous terrain, part I, A numerical and observational comparison, *Mon. Weather Rev.*, *122*, 1449-1471, 1994a.

Bossert, J. E., and W. R. Cotton, Regional-scale flows in mountainous terrain, part II, Simplified numerical experiments, *Mon. Weather Rev.*, *122*, 1472-1489, 1994b.

Bravo, J. L., M. T. Diaz, C. Gay, and J. Fajardo, A short term prediction model for surface ozone at southwest part of Mexico valley, *Atmósfera*, *9*, 33-45, 1996.

Chen, S., and W. R. Cotton, A one-dimensional simulation of the stratocumulus-capped mixed layer, *Boundary Layer Meteorol.*, *25*, 289-321, 1983.

Collins, C. O., and S. L. Scott, Air Pollution in the valley of Mexico, *Geogr. Rev.*, *83*, 119-133, 1993.

de Wekker, S. F. J., S. Zhong, J. D. Fast, and C. D. Whiteman, A numerical study of the thermally driven plain-to-basin wind over idealized basin topographies, *J. Appl. Meteorol.*, *37*, 606-622, 1998.

Díaz-Francés, E., M. E. Ruíz, and G. Sosa, Spatial stratification and multivariate analyses of Mexico City air pollution data, in

Proceedings of the 2nd International Conference on Air Pollution, pp. 361-370, Comput. Mech. Publ., Billerica, Mass., 1994.

Dickinson, R. E., A. Henderson-Sellers, P. J. Kennedy, and M. F. Wilson, Biosphere-Atmosphere Transfer Scheme (BATS) for the NCAR Community Climate Model, *NCAR Tech. Note, NCAR/TN-275 +STR*, 69 pp., Nat. Cent. for Atmos. Res., Boulder, Colo., 1986.

Doran, J. C., et al., The IMADA-AVER boundary-layer experiment in the Mexico City area, *Bull. Am. Meteorol. Soc.*, *79*, 2497-2508, 1998.

Edgerton, S. A., et al., Particulate air pollution in Mexico City: A collaborative research project, *J. Air Waste Manage. Assoc.*, *49*, 1221-1229, 1999.

Fast, J. D., Mesoscale modeling in areas of highly complex terrain, *J Appl. Meteorol.*, *34*, 2762-2782, 1995.

Fast, J. D., Air pollutant transport within the Mexico City basin, paper presented at 7th International Conference on Air Pollution, Wessex Inst. of Technol., 27-29 July 1999, San Francisco, Calif., 1999.

Fast, J. D., and S. Zhong, Meteorological factors associated with inhomogeneous ozone concentrations within the Mexico City basin, *J. Geophys. Res.*, *103*, 18,927-18,946, 1998.

Fast, J. D., S. Zhong, and C. D. Whiteman, Boundary layer evolution within a canyonland basin, part II, Numerical simulations of nocturnal flows and heat budgets, *J. Appl. Meteorol.*, *35*, 2162-2178, 1996.

Fitzjarrald, D. R., Slope winds in Veracruz, *J. Clim. Appl. Meteorol.*, *25*, 133-144, 1986.

Garfias, J., and R. González, Air quality in Mexico City, chap. 7, in *The Science of Global Change: The Impact of Human Activities*, ACS Symp. Ser., edited by D. A. Dunnette and R. J. O'Brien, pp. 149-161, Am. Chem. Soc., Washington, D.C., 1992.

Guzmán, F., and G. E. Streit, Mexico City air quality research initiative, in *Air Pollution '93*, edited by P. Zannetti, C. A. Brebbia, J. E. Garcia Gardea, and G. A. Milian, pp. 599-609, Comput. Mech. Publ., Billerica, Mass., 1993.

Jauregui, E., The urban climate of Mexico City, *Erdkunde*, *27*, 298-307, 1973.

Jauregui, E., Local wind and air pollution interaction in the Mexico Basin, *Atmósfera*, *1*, 131-140, 1988.

Jauregui, E., Mexico City's urban heat island revisited, *Erdkunde*, *47*, 185-195, 1993.

Jauregui, E., Heat island development in Mexico City, *Atmos. Environ.*, *31*, 3821-3831, 1997.

Kimura, F., and T. Kuwagata, Thermally induced wind passing from plain to basin over a mountain range, *J. Appl. Meteorol.*, *32*, 1538-1547, 1993.

Louis, J. F., A parametric model of vertical eddy fluxes in the atmosphere, *Boundary Layer Meteorol.*, *17*, 187-202, 1979.

Mellor, G. L., and T. Yamada, Development of a turbulent closure model for geophysical fluid problems, *Rev. Geophys.*, *20*, 851-875, 1982.

Miller, P. R., M. de Lourdes de Bauer, A. Q. Nolasco, and T. H. Tejeda, Comparison of ozone exposure characteristics in forested regions near Mexico City and Los Angeles, *Atmos. Environ.*, *28*, 141-148, 1994.

Nickerson, E. C., G. Sosa, H. Hochstein, P. McCaslin, W. Luke, and A. Schanot, Project AGUILA: In situ measurements of Mexico City air pollution by a research aircraft, *Atmos. Environ.*, *26*(B), 445-451, 1992.

Oke, T. R., G. Zeuner, and E. Jauregui, The surface energy balance in Mexico City, *Atmos. Environ.*, *26*(B), 433-444, 1992.

Oke, T. R., R. A. Spronken-Smith, E. Jauregui, and C. S. B. Grimmond, The energy balance of central Mexico City during the dry season, *Atmos. Environ.*, *33*, 3919-3930, 1999.

Pielke, R. A., et al., A comprehensive meteorological modeling system—RAMS, *Meteorol. Atmos. Phys.*, *49*, 69-91, 1992.

Raga, G. B., and L. Le Moyne, On the nature of air pollution dynamics in Mexico City, I, Nonlinear analysis, *Atmos. Environ.*, *30*, 3987-3993, 1996.

Steinacker, R., Area-height distribution of a valley and its relation to the valley wind, *Contrib. Atmos. Phys.*, *57*, 64-71, 1984.

Stull, R. B., *An Introduction to Boundary Layer Meteorology*, 666 pp., Kluwer Acad., Norwell, Mass., 1988.

Tremback, C. J., and R. Kessler, A surface temperature and moisture parameterization for use in mesoscale numerical models, in *Preprints, 7th Conference on Numerical Weather Prediction*, pp. 355-358, Am. Meteorol. Soc., Boston, Mass., 1985.

Varela, J. R., Photochemical modeling of pollution scenarios in Mexico City, chap. 5, in *Urban Air Pollution*, edited by H. Power, N. Moussiopoulos, and C. A. Brebbia, Comput. Mech. Publ., *1*, 159-186, 1994.

Wang, W., and T. T. Warner, Use of four-dimensional data assimilation by Newtonian relaxation and latent-heat forcing to improve a mesoscale-model precipitation forecast: A case study, *Mon. Weather Rev.*, *116*, 2593-2613, 1988.

Whiteman, C. D., Observations of thermally developed wind systems in mountainous terrain, chap. 2, in *Atmospheric Processes Over Complex Terrain*, *Meteorol. Monogr.*, vol. 23, edited by W. Blumen, pp. 5-42, Am. Meteorol. Soc., Boston, Mass., 1990.

Whiteman, C. D., and K. J. Allwine, Extraterrestrial solar radiation on inclined surfaces, *Environ. Software*, *1*, 164-169, 1986.

Whiteman, C. D., T. B. McKee, and J. C. Doran, Boundary layer evolution within a canyonland basin, part I, Mass, heat and moisture budgets from observations, *J. Appl. Meteorol.*, *35*, 2145-2161, 1996.

Whiteman, C. D., X. Bian, and S. Zhong, Wintertime evolution of the temperature inversion in the Colorado Plateau Basin, *J. Appl. Meteorol.*, *38*, 1103-1117, 1999a.

Whiteman, C. D., S. Zhong, and X. Bian, Wintertime boundary-layer structure in the Grand Canyon, *J. Appl. Meteorol.*, *38*, 1084-1102, 1999b.

Williams, M. D., M. J. Brown, X. Cruz, G. Sosa, and G. Streit, Development and testing of meteorology and air dispersion models for Mexico City, *Atmos. Environ.*, *29*, 2929-2960, 1995.

Zdunkowski, W. G., R. M. Welch, and J. Paegle, One-dimensional numerical simulation of the effects of air pollution on the planetary boundary layer, *J. Atmos. Sci.*, *33*, 2399-2414, 1976.

Zhong, S., and J. C. Doran, Thermally driven winds into the Mexico City basin through a mountain gap, in *Preprints, 8th Conference on Mountain Meteorology*, pp. 426-431, Am. Meteorol. Soc., Boston, Mass., 1998.

X. Bian, J. C. Doran, J. D. Fast, C. D. Whiteman, and S. Zhong, Pacific Northwest National Laboratory, P.O. Box 999, MSIN K9-30, Richland, WA 99352. (randy.x.bian@pnl.gov; christopher.doran@pnl.gov; jerome.fast@pnl.gov; dave.whiteman@pnl.gov; shiyuan.zhong@pnl.gov)

(Received May 28, 1999; revised December 10, 1999; accepted December 18, 1999.)